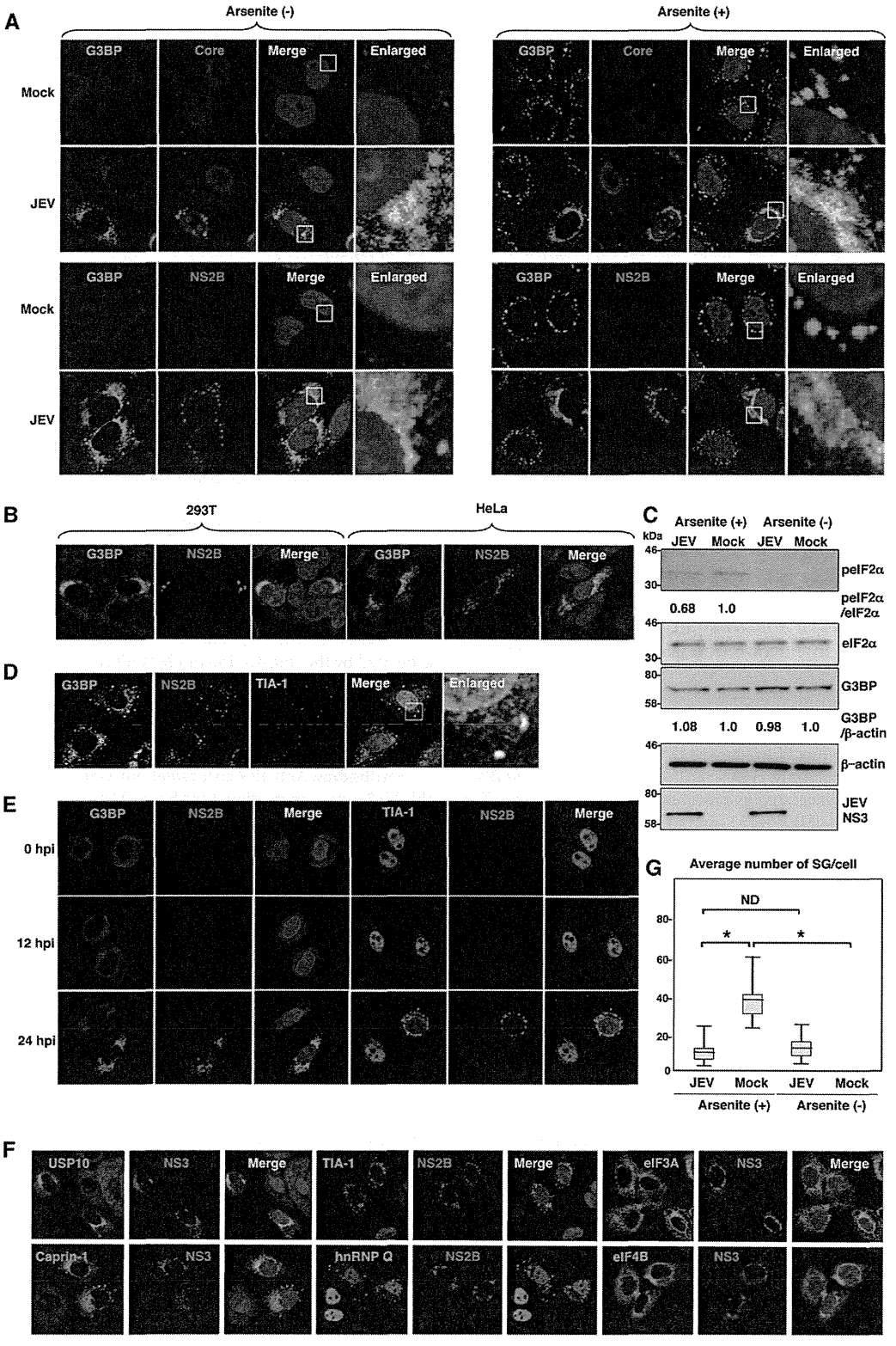

FIG 1 Dynamics of SG-associated factors during JEV infection. (A) Huh7 cells infected with JEV at an MOI of 0.5 were treated with or without 1.0 mM sodium arsenite for 30 min at 37°C, and the levels of expression of G3BP and JEV core protein/NS2B were determined at 24 h postinfection by immunofluorescence analysis with mouse anti-G3BP MAb and rabbit anti-core protein or anti-NS2B PAb, followed by AF488-conjugated anti-mouse IgG (Invitrogen) and AF594-conjugated anti-rabbit IgG, respectively. Cell nuclei were stained with DAPI (blue). (B) Cellular localizations of G3BP and JEV NS2B in 293T and HeLa cells infected with JEV were determined at 24 h postinfection by immunofluorescence analysis with mouse anti-G3BP MAb and rabbit anti-NS2B PAb, followed by AF488-conjugated anti-mouse IgG and AF594-conjugated anti-rabbit IgG, respectively. Cell nuclei were stained with DAPI (blue). (C) Phosphorylation of eIF2α in cells prepared as described in panel A was determined by immunoblotting using the indicated antibodies. The band intensities were quantified by ImageJ

a single-stranded positive-sense RNA genome of approximately 11 kb. The genomic RNA carries a single large open reading frame, and a polyprotein translated from the genome is cleaved co- and posttranslationally by host and viral proteases to yield three structural proteins, the core, precursor membrane (PrM), and envelop (E) proteins, and seven nonstructural (NS) proteins, NS1, NS2A, NS2B, NS3, NS4A, NS4B, and NS5 (13). PrM is further cleaved by the multibasic protease, furin, and matured to membrane (M) protein. The core, M, and E proteins are components of extracellular mature virus particles. NS proteins are not incorporated into particles and are thought to be involved in viral replication, which occurs in close association with ER-derived membranes (14). Previous reports have shown that WNV and DENV inhibit SG formation by sequestering TIA-1 and TIAR through specific interaction with viral RNA (15, 16). In addition, the membrane structure induced by WNV infection was suggested to prevent PKR activation and avoid induction of SG formation (17). In this study, we show that JEV core protein plays an important role in inhibition of SG formation. JEV core protein recruited several SG-associated proteins, including G3BP and USP10, through an interaction with Caprin-1 and suppressed SG formation. Furthermore, a mutant JEV carrying a core protein incapable of binding to Caprin-1 exhibited lower propagation *in vitro* and lower pathogenicity in mice than the wild-type (WT) JEV, suggesting that inhibition of SG formation by the core protein is crucial to antagonize host defense. These results reveal a novel strategy of JEV to inhibit SG formation through an interaction with Caprin-1 and facilitate viral propagation.

MATERIALS AND METHODS

Plasmids. Plasmids encoding FLAG-tagged JEV core protein (pCAGPM-FLAG-Core) and hemagglutinin (HA)-tagged JEV proteins (pCAGPM-HA-JEV proteins) were generated as previously described (18, 19). The cDNA of the core protein of JEV AT31 (amino acid residues 2 to 105) was amplified from the pCAGPM-FLAG-Core plasmid by PCR and cloned into pET21b (Novagen-Merck, Darmstadt, Germany) for expression in bacteria as a His-tagged protein and in pCAG-MCS2-FOS for expression in mammalian cells as a FLAG-One-STrEP (FOS)-tagged protein. The resulting plasmids were designated pET21b-Core-His and pCAG-Core-FOS, respectively. The cDNA of the core protein of DENV2 (amino acid residues 2 to 100) was amplified from the pCAG/FLAG-DEN2C-HA plasmid (19) by PCR and cloned into pCAGPM-N-FLAG. The cDNA of human Caprin-1 was amplified from 293T cells by reverse transcription-PCR (RT-PCR) and cloned into pCAGPM-N-HA (20) and pGEX 6P-1 (GE Healthcare, Buckinghamshire, United Kingdom) for expression in bacteria as a glutathione *S*-transferase (GST) fusion protein and designated pCAGPM-HA-Caprin-1 and pGEX-GST-Caprin-1, respectively. The cDNAs of human G3BP1 and USP10 were also amplified from 293T cells by RT-PCR and cloned into pCAGPM-N-HA. The nucleotide residues of the adenine at 384, adenine at 385, cytosine at 387, and guanine at 388 of the JEV genome in pMWATG1 were replaced with guanine, cytosine, guanine, and cytosine, respectively, by PCR-based mutagenesis to change Lys^{97} and Arg^{98} of the core protein to Ala, yielding pMWAT/KR9798A. The cDNA of the mutant core protein was also cloned into pCAGPM-N-FLAG and pET21b. To generate stable cell lines expressing *Aequorea coerulescens* green fluorescent protein (AcGFP)-fused Caprin-1, the cDNA of human Caprin-1 was amplified by RT-PCR and cloned into pAcGFP N1 (Clontech, Mountain View, CA), and the Caprin-1-AcGFP gene was subcloned into the lentiviral vector pCSII-EF-RfA (21) and designated pCSII-EF-Caprin-1-AcGFP. All plasmids were confirmed by sequencing with an ABI Prism 3130 genetic analyzer (Applied Biosystems, Tokyo, Japan).

Cells and stress treatment. Mammalian cell lines, Vero (African green monkey kidney), 293T (human kidney), Huh7 (human hepatocellular carcinoma), and HeLa (human cervical carcinoma), were maintained in Dulbecco's modified Eagle's minimal essential medium (DMEM) (Sigma, St. Louis, MO) supplemented with 100 U/ml penicillin, 100 mg/ml streptomycin, nonessential amino acids (Sigma), and 10% fetal bovine serum (FBS). The mosquito cell line C6/36 (*Aedes albopictus*) was grown in Leibovitz's L-15 medium with 10% FBS. Huh7 cells were transduced with a lentiviral vector expressing Caprin-1-AcGFP and AcGFP and designated Huh7/Caprin-1-AcGFP and Huh7/AcGFP, respectively. For induction of SGs, cells were treated with sodium arsenite at a final concentration of 1.0 mM in the culture medium for 30 min prior to fixation or lysis of the cells. SG formation was defined morphologically by immunostaining using anti-SG-related factor antibodies described below. Cell viability was determined by using CellTiter-Glo (Promega, Madison, WI) according to the manufacturer's instruction.

Viruses. The wild-type and 9798A mutant of the JEV AT31 strain were generated by the transfection of pMWATG1 and pMWAT/KR9798A, respectively, as described previously (22). Viral infectivity was determined by an immunostaining focus assay as described previously (20), and the results are expressed in focus-forming units (FFU). JEV and DENV serotype 2 New Guinea C strain were amplified in C6/36 cells.

Antibodies. Anti-JEV core rabbit polyclonal antibody (PAb) and anti-JEV NS3 mouse monoclonal antibody (MAb) were prepared as described previously (20, 23). Anti-JEV NS2B rabbit PAb was generated with synthetic peptides of JEV NS2B at Scrum, Inc. (Tokyo, Japan). Anti-DENV core protein rabbit PAb was prepared by using a GST-fused recombinant protein containing amino acid residues 2 to 100 of the DENV core protein. Anti-FLAG mouse MAb (M2) and rabbit PAb and anti-β-actin mouse MAb were purchased from Sigma. Anti-hnRNP Q mouse MAb (ab10687), anti-USP10 rabbit PAb (ab70895), and anti-eIF4B rabbit PAb (ab78916) were purchased from Abcam (Cambridge, United Kingdom). Anti-eIF2α, anti-phospho-eIF2α, and anti-eIF3A rabbit PAbs were purchased from Cell Signaling Technology (Danvers, MA). Anti-HA mouse MAb (HA11), anti-HA rat MAb (3F10), anti-His mouse MAb, anti-GFP mouse MAb (JL-8), anti-JEV envelope protein mouse MAb (6B4A-10), anti-G3BP mouse MAb, anti-TIA-1 goat PAb, anti-Caprin-1 rabbit PAb, and anti-dsRNA mouse MAb were purchased from Covance (Richmond, CA), Roche (Mannheim, Germany), R&D Systems (Minneapolis, MN), Clontech, Chemicon (Temecula, CA), BD Biosciences (Franklin Lakes, NJ), Santa Cruz (Santa Cruz, CA), Proteintech (Chicago, IL), and Bio-

software (NIH, Bethesda, MD), and the relative levels for the indicated proteins are shown based on the level of the mock-infected cells. (D) Cellular localizations of G3BP, NS2B, and TIA-1 in Huh7 cells infected with JEV were determined at 24 h postinfection by immunofluorescence analysis with mouse anti-G3BP MAb, rabbit anti-NS2B PAb, and goat anti-TIA-1 PAb, followed by AF488-conjugated anti-mouse IgG, AF594-conjugated anti-rabbit IgG, and AF633-conjugated anti-goat IgG, respectively. Cell nuclei were stained with DAPI (gray). (E) Dynamics of G3BP and TIA-1 during JEV infection. Huh7 cells infected with JEV were immunostained at 0, 12, and 24 h postinfection (hpi) with mouse anti-G3BP MAb or goat anti-TIA-1 PAb and rabbit anti-NS2B PAb, followed by AF488-conjugated anti-mouse IgG or AF488-conjugated anti-goat IgG and AF594-conjugated anti-rabbit IgG, respectively. Cell nuclei were stained with DAPI (blue). (F) Cellular localization of SG-associated proteins (USP10, Caprin-1, TIA-1, hnRNP Q, eIF3A, and eIF4B) (green, AF488-conjugated secondary antibody) and JEV NS2B/NS3 (red, AF-594-conjugate secondary antibody) in Huh7 cells infected with JEV was determined by immunoblotting at 24 h postinfection. Cell nuclei were stained with DAPI (blue). (G) Numbers of G3BP-positive foci in 30 cells prepared as described in panel A were counted for each experimental condition. Lines, boxes, and error bars indicate the means, 25th to 75th percentiles, and 95th percentiles, respectively. The significance of differences between the means was determined by a Student's *t* test.*, $P < 0.01$; ND, no significant difference.

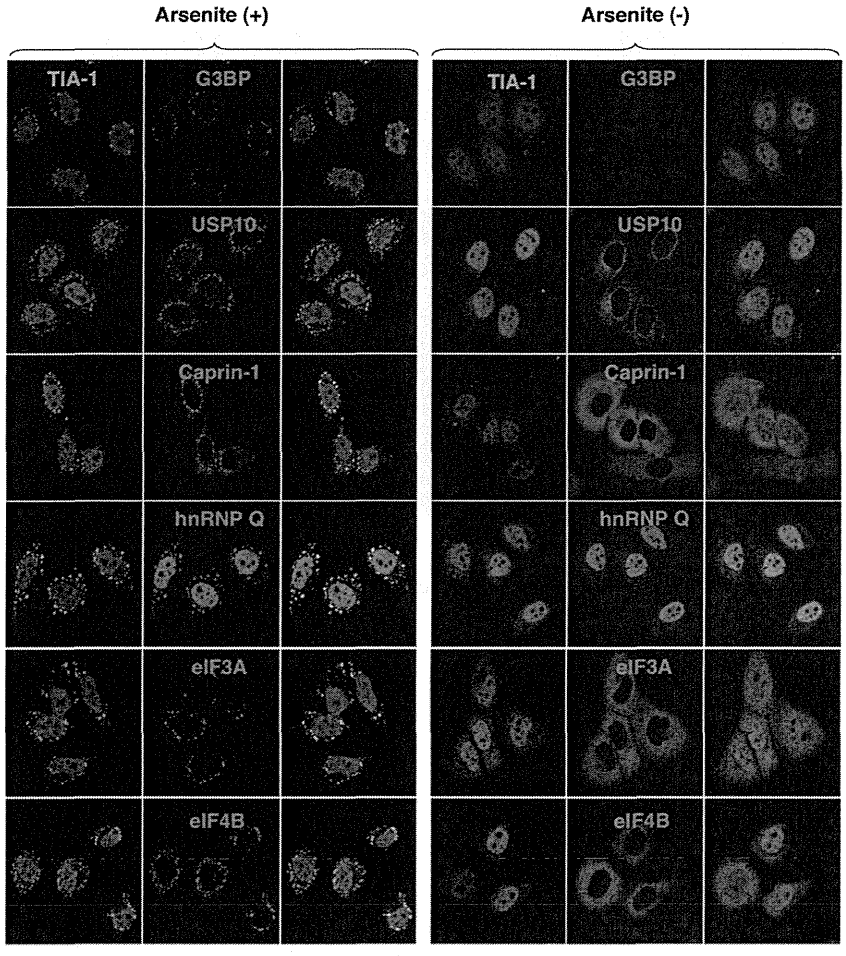

FIG 2 Each SG-associated factor forms SGs under oxidative stress. After treatment with 1.0 mM sodium arsenite for 30 min at 37°C, Huh7 cells were subjected to immunofluorescence analysis with the indicated primary antibodies, followed by AF488-conjugated anti-goat IgG and AF594-conjugated anti-mouse or rabbit IgG. Cell nuclei were stained with DAPI (blue).

center (Szirak, Hungary), respectively. Alexa Fluor (AF)-conjugated secondary antibodies were purchased from Invitrogen (Carlsbad, CA).

Immunofluorescence microscopy. Huh7 cells were fixed in 4% paraformaldehyde in phosphate-buffered saline (PBS) for 15 min at room temperature. After cells were quenched for 10 min with PBS containing 50 mM ammonium chloride (NH_4Cl), they were permeabilized with 0.2% Triton X-100 in PBS for 10 min and blocked with PBS containing 2% bovine serum albumin (BSA) for 30 min at room temperature. The cells were then incubated with the antibodies indicated in the figure legends. Nuclei were stained with 4′,6′-diamidino-2-phenylindole (DAPI). The samples were examined by a Fluoview FV1000 laser scanning confocal microscope (Olympus, Tokyo, Japan).

Transfection, immunoprecipitation, and immunoblotting. Plasmids were transfected into 293T or Huh7 cells by use of TransIT LT1 (Mirus, Madison, WI), and cells collected at 24 h posttransfection were subjected to immunostaining, immunoprecipitation, and/or immunoblotting as described previously (24). The immunoprecipitates were boiled in sodium dodecyl sulfate (SDS) sample buffer and subjected to SDS-polyacrylamide gel electrophoresis (SDS-PAGE). The proteins were transferred to polyvinylidene difluoride membranes (Millipore, Bedford, MA) and incubated with the appropriate antibodies. The immune complexes were visualized with SuperSignal West Femto substrate (Thermo Scientific, Rockford, IL) and detected by use of an LAS-3000 image analyzer system (Fujifilm, Tokyo, Japan).

FOS-tagged purification and mass spectrometry. pCAG-Core-FOS or empty vector was transfected into 293T cells, harvested at 24 h posttransfection, washed with cold PBS, suspended in cell lysis buffer (20 mM Tris-HCl, pH 7.4, 135 mM NaCl, 1% Triton X-100, and protease inhibitor cocktail [Complete; Roche]), and centrifuged at 14,000 × *g* for 20 min at 4°C. The supernatant was pulled down using 50 μl of STrEP-Tactin Sepharose (IBA, Gottingen, Germany) equilibrated with cell lysis buffer for 2 h at 4°C. The affinity beads were washed three times with cell lysis buffer and suspended in 2× SDS-PAGE sample buffer. The proteins were subjected to SDS-PAGE, followed by Coomassie brilliant blue (CBB) staining using CBB Stain One (Nakalai Tesque, Kyoto, Japan). The gels were divided into 10 pieces, and each fraction was trypsinized and subjected to liquid chromatography-tandem mass spectrometry (LC-MS/MS) analysis to identify coimmunoprecipitated proteins. All of the proteins in gels were identified comprehensively, and the proteins detected in cells transfected with pCAG-Core-FOS but not in those with empty vector were regarded as candidates for binding partners of JEV core.

Gene silencing. A commercially available small interfering RNA (siRNA) pool targeting Caprin-1 (siGENOME SMARTpool, human Caprin1) and control nontargeting siRNA were purchased from Dharmacon (Buckinghamshire, United Kingdom) and transfected into 293T cells using Lipofectamine RNAiMAX (Invitrogen) according to the manufacturer's protocol.

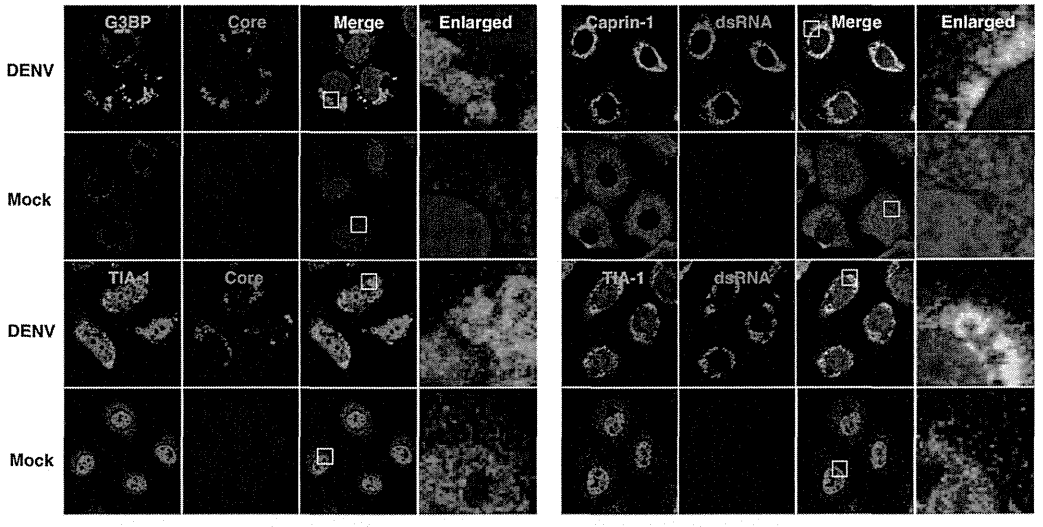

FIG 3 Subcellular localizations of the SG-associated proteins during DENV infection. Cellular localizations of G3BP, Caprin-1, and TIA-1 (green, AF488-conjugated secondary antibody) and viral components (core protein and dsRNA) (red, AF-594-conjugate secondary antibody) in Huh7 cells infected with DENV were determined by immunofluorescence analysis using the appropriate antibodies at 48 h postinfection. Cell nuclei were stained with DAPI (blue).

Preparation of recombinant proteins and GST pulldown assay. His-tagged JEV core protein (core-His) was purified as described in a previous report (25). Briefly, core-His was expressed in *Escherichia coli* (*E. coli*) Rosetta-gami 2(DE3) strain cells (Novagen-Merck) transformed with pET21b-Core-His (WT or 9798A). Bacteria grown to an optical density at 600 nm of 0.6 were induced with 0.5 mM isopropyl-β-D-thiogalactopyranoside (IPTG), incubated for 5 h at 37°C with shaking, collected by centrifugation at 6,000 × *g* for 10 min, lysed in 10 ml of bacteria lysis buffer (50 mM Tris-HCl, pH 7.4, 150 mM NaCl, 1 mM EDTA, 1% Triton X-100, and protease inhibitor cocktail [Complete; Roche]) by sonication on ice, and centrifuged at 10,000 × *g* for 15 min. The supernatant containing core-His was subjected to ammonium sulfate fractionation, followed by cation exchange chromatography with a HiTrap SP column (GE Healthcare). The eluted core-His recombinant protein was dialyzed with 50 mM Tris-HCl buffer containing 150 mM NaCl at 4°C overnight. GST-fused Caprin-1 (GST-Caprin-1) was expressed in *E. coli* BL21(DE3) cells transformed with pGEX-GST-Caprin-1. Bacteria grown to an optical density at 600 nm of 1.0 were induced with 0.1 mM IPTG, incubated for 5 h at 25°C with shaking, collected by centrifugation at 6,000 × *g* for 10 min, lysed in 10 ml of bacteria lysis buffer by sonication on ice, and centrifuged at 10,000 × *g* for 15 min. The supernatant was mixed with 200 μl of glutathione-Sepharose 4B beads (GE Healthcare) equilibrated with bacteria lysis buffer for 1 h at room temperature, and then the beads were washed five times with lysis buffer. Twenty micrograms of GST-Caprin-1 or GST was mixed with equal volumes of the purified core-His for 2 h at 4°C with gentle agitation. The beads were washed five times with bacteria lysis buffer and then suspended in SDS-PAGE sample buffer.

Mouse experiments. Experimental infections were approved by the Committee for Animal Experiment of RIMD, Osaka University (H19-2-0). Female ICR mice (3 weeks old) were purchased from CLEA Japan (Tokyo, Japan) and kept in specific pathogen-free environments. Groups of mice ($n = 10$) were intraperitoneally inoculated with 5×10^4 FFU (100 μl) of the viruses. The mice were observed for 3 weeks after inoculation to determine survival rates. To examine viral growth in the brain, 5×10^4 FFU of the viruses were intraperitoneally administered to the groups of mice ($n = 3$). At 7 days postinfection, mice were euthanized, and the cerebrums were collected. The infectious titers in the homogenates of the cerebrums were determined in Vero cells as described above.

RESULTS

JEV infection confers resistance to SG induction. To examine the formation of SGs in cells infected with JEV, Huh7 cells were infected with JEV at a multiplicity of infection (MOI) of 0.5, and the expression of JEV proteins and an accepted marker for SGs, G3BP, was determined by immunofluorescence analysis at 24 h postinfection. G3BP was mainly accumulated in the perinuclear region and partially colocalized with the JEV core protein, while only partial colocalization with the NS2B protein was also observed (Fig. 1A, left). In addition, a few small G3BP-positive foci were scattered in the cytoplasm. This accumulation of G3BP was observed in not only Huh7 cells but also other cell lines, i.e., 293T and HeLa cells, infected with JEV (Fig. 1B). However, the expression level of G3BP in cells infected with JEV was comparable to that in mock-infected cells (Fig. 1C). To further investigate SG induction by JEV infection, expression of TIA-1, another SG marker, was examined. Although accumulation of TIA-1 in the perinuclear region was not observed, a few TIA-1-positive foci were observed in the JEV-infected cells and were colocalized with G3BP and JEV NS2B, indicating that SG foci were induced in cells infected with JEV (Fig. 1D). The accumulation of G3BP and the aggregation of TIA-1, indicating SG formation, appeared at 24 h postinfection in accord with the expression of viral proteins (Fig. 1E). We further examined the dynamics of other SG-associated factors in cells infected with JEV. Each factor formed clear SGs in cells treated with sodium arsenite, a potent SG inducer eliciting oxidative stress (Fig. 2). As shown in Fig. 1F, three distinct patterns of the subcellular localization of SG components were observed. USP10 and Caprin-1 were accumulated in the perinuclear region and also formed a few small foci scattered throughout the cytoplasm, as seen for G3BP; TIA-1 and hnRNP Q formed cytoplasmic foci but were not accumulated in the perinuclear region; and subcellular localization of eIF3A and eIF4B was not changed. The cytoplasmic foci were confirmed as SGs by immunofluorescence analyses using specific antibodies to SG-associated factors (data not shown). Taken together, these results indicate that JEV infection induces accumulation of several RBPs and formation of a few SGs.

It has been shown previously that infection with WNV or DENV confers resistance to SG formation induced by sodium arsenite (15). To determine the effect of JEV infection on the SG

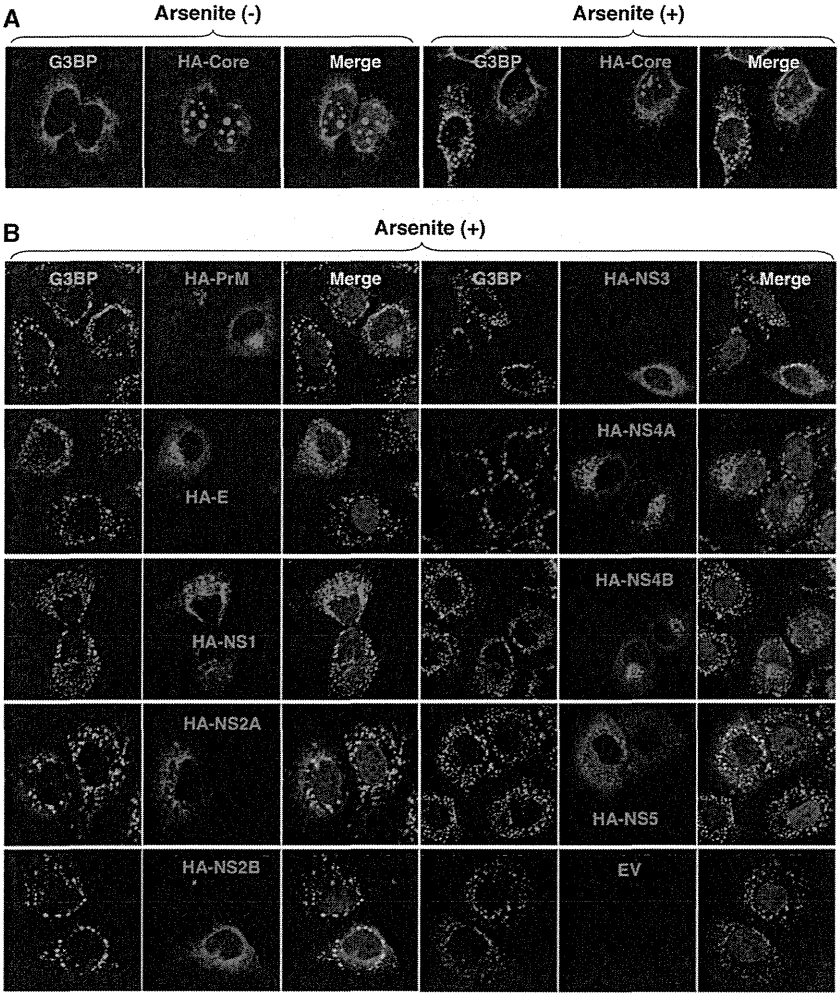

FIG 4 Inhibition of the arsenite-induced SG formation by the expression of JEV proteins. (A) Huh7 cells transfected with a plasmid, pCAGPM-HA-Core, were treated with or without 1.0 mM sodium arsenite for 30 min at 37°C, and the cellular localizations of G3BP and HA-Core were determined at 24 h posttransfection by immunofluorescence analysis with mouse anti-G3BP MAb and rat anti-HA MAb, followed by AF488-conjugated anti-mouse IgG and AF594-conjugated anti-rat IgG, respectively. Cell nuclei were stained with DAPI (blue). (B) Huh7 cells, which were separately transfected with a plasmid expressing an individual viral protein (pCAGPM-HA-JEV protein) as indicated in the figure, were treated with 1.0 mM sodium arsenite for 30 min at 37°C and subjected to an immunofluorescence assay using mouse anti-G3BP MAb and rat anti-HA MAb, followed by AF488-conjugated anti-mouse IgG and AF594-conjugated anti-rat IgG, respectively. Cell nuclei were stained with DAPI (blue).

formation induced by sodium arsenite, JEV-infected cells were treated with 0.5 mM sodium arsenite for 30 min at 24 h postinfection. Although many G3BP-positive foci were observed in mock-infected cells by the treatment with sodium arsenite, accumulation of G3BP in the perinuclear region was observed in the JEV-infected cells (Fig. 1A, right), and the numbers of G3BP-positive foci in the JEV-infected cells were less than those in the mock-infected cells (Fig. 1G). Although it has been reported that a significant reduction of the phosphorylation at Ser^{51} of eIF2α in cells treated with arsenite was induced by infection with WNV (15), the phosphorylation of eIF2α was slightly suppressed in the JEV-infected cells (Fig. 1C). Furthermore, while previous studies reported that Caprin-1 and TIA-1 were colocalized with dsRNA in cells infected with DENV (15, 26), no colocalization of G3BP or TIA-1 with the DENV core protein was observed in the present study (Fig. 3), suggesting that the mechanisms of the viral circumvention of SG formation in cells infected with JEV are different from those in cells infected with WNV and DENV.

JEV core protein suppresses SG formation induced by sodium arsenite. To elucidate the molecular mechanisms of suppression of SG formation induced by sodium arsenite during JEV infection, we tried to identify which viral protein(s) is responsible for the SG inhibition. Since G3BP was colocalized with JEV core protein, we first examined the involvement of the core protein in the perinuclear accumulation of G3BP and in the suppression of SG formation. The expression of JEV core protein alone induced the accumulation of G3BP in the perinuclear region (Fig. 4A, left panel) and suppressed sodium arsenite-induced SG formation (Fig. 4A, upper right cell in the right panel), similarly to JEV infection. In contrast, inhibition of SG formation induced by sodium arsenite was not observed in cells expressing other JEV proteins (Fig. 4B). These results suggest that JEV core protein is responsible for the circumvention of the SG formation observed in cells infected with JEV.

JEV core protein directly interacts with Caprin-1, an SG-associated cellular factor. Since JEV core protein was suggested to

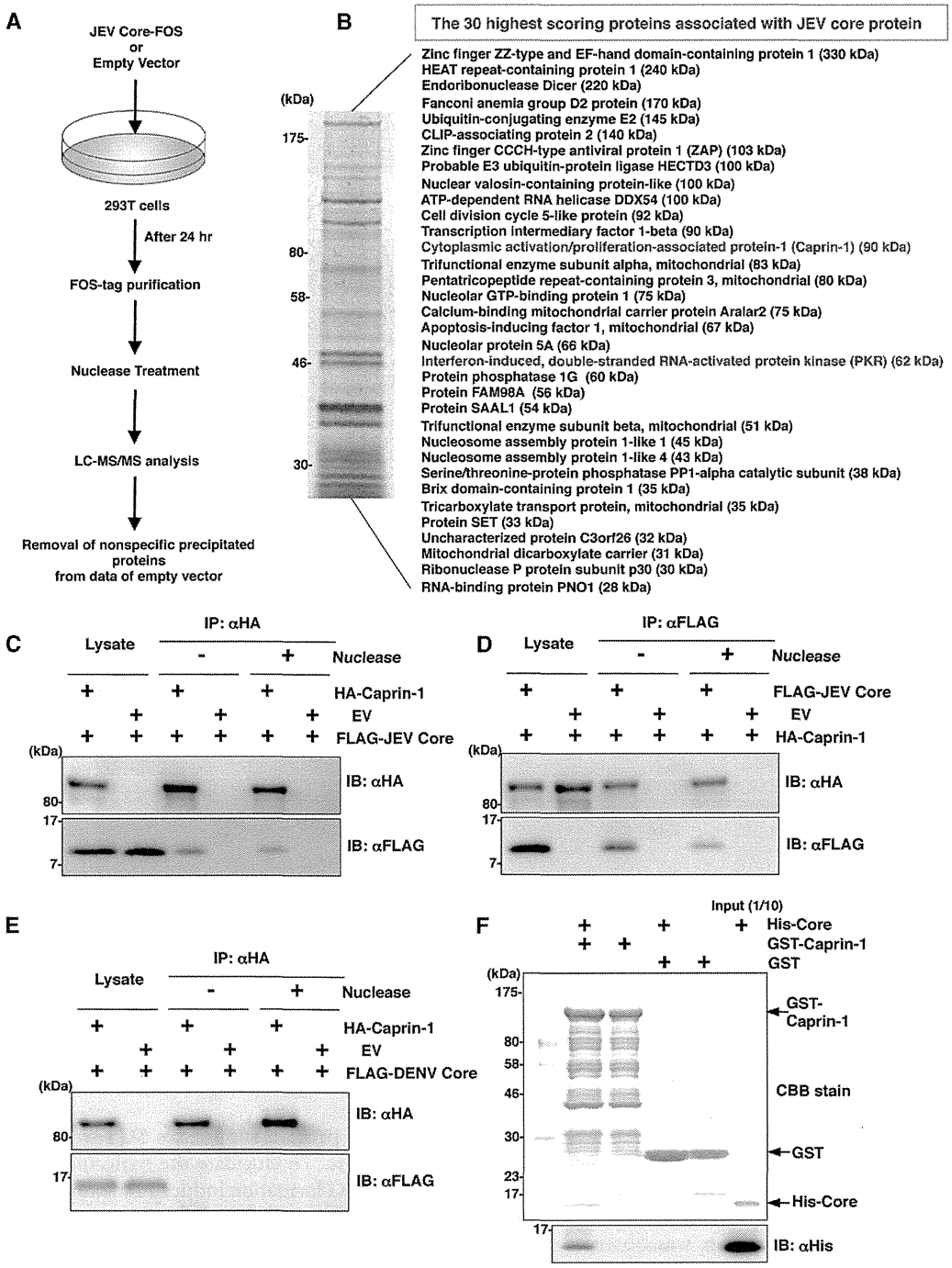

FIG 5 JEV core protein directly interacts with Caprin-1, an SG-associated cellular factor. (A) Identification of host cellular proteins associated with JEV core protein by FOS-tagged purification and LC-MS/MS analysis. Overview of the FOS-tagged purification of cellular proteins associated with JEV core protein. (B) The 30 candidate proteins as binding partners of JEV core protein exhibiting high scores are listed. PKR and Caprin-1 are indicated in red. (C and D) FLAG-JEV core protein and HA-Caprin-1 were coexpressed in 293T cells, and the cell lysates harvested at 24 h posttransfection were treated with or without micrococcal nuclease for 30 min at 37°C and immunoprecipitated (IP) with anti-HA (αHA) or anti-FLAG (αFLAG) antibody, as indicated. The precipitates were subjected to immunoblotting (IB) to detect coprecipitated counterparts. (E) FLAG-DENV core protein was coexpressed with HA-Caprin-1 in 293T cells, immunoprecipitated with anti-HA antibody, and immunoblotted with anti-HA or anti-FLAG antibody. (F) His-tagged JEV core protein was incubated with either GST-fused Caprin-1 or GST for 2 h at 4°C, and the precipitates obtained by GST pulldown assay were subjected to CBB staining and immunoblotting with anti-His antibody.

participate in the inhibition of SG formation, we tried to identify cellular factors associated with the core protein by LC-MS/MS analysis, as shown in Fig. 5A. Among the 30 factors with the best scores, two SG-associated proteins, PKR (Mascot search score, 206) and Caprin-1 (Mascot search score, 153), were identified as binding partners of JEV core protein (Fig. 5B). Although PABP1, hnRNP Q, Staufen, G3BP, and eIF4G were also identified, their scores were lower than those of PKR and Caprin-1. Because the

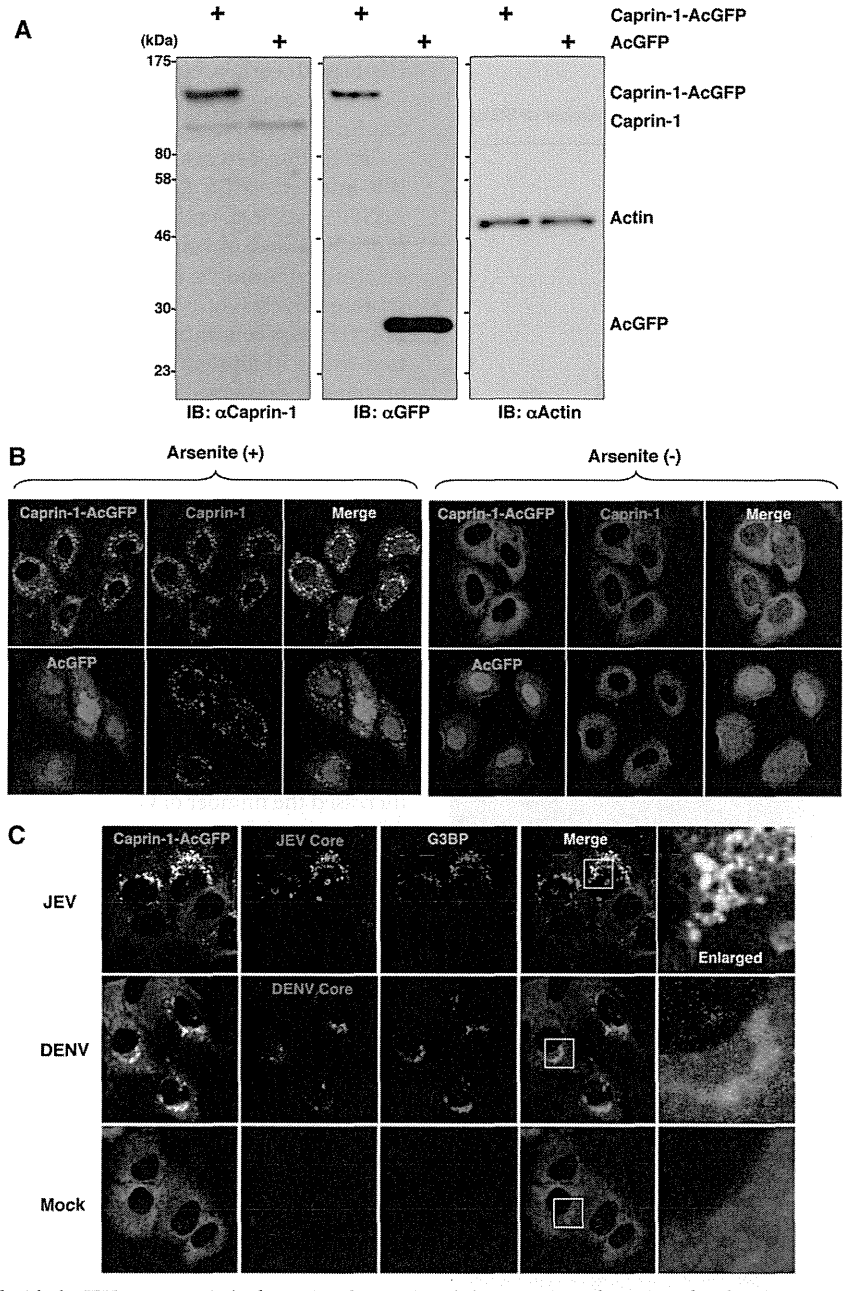

FIG 6 Caprin-1 is colocalized with the JEV core protein in the perinuclear region. (A) Expression of Caprin-1 fused with AcGFP (Caprin-1-AcGFP), Caprin-1, actin, or AcGFP in lentivirally transduced Huh7 cells was determined by immunoblotting using the appropriate antibodies. (B) Subcellular localization of Caprin-1-AcGFP or AcGFP (green) and endogenous Caprin-1 (red) in cells treated with/without 1.0 mM sodium arsenite for 30 min at 37°C was determined by immunofluorescence assay with rabbit anti-Caprin-1 PAb and AF594-conjugated anti-rabbit IgG. Cell nuclei were stained with DAPI (blue). (C) Huh7/Caprin-1-AcGFP cells were infected with either JEV or DENV at an MOI of 0.5, and the cellular localizations of JEV and DENV core (red) with Caprin-1-AcGFP and G3BP (blue) were determined at 24 h and 48 h postinfection, respectively. Cells were stained with mouse anti-G3BP MAb and rabbit anti-JEV or DENV core protein PAb, followed by AF633-conjugated anti-mouse IgG and AF594-conjugated anti-rabbit IgG, respectively, and examined by immunofluorescence analysis.

results shown in Fig. 1B suggest that the inhibition of SG formation takes place downstream of eIF2α phosphorylation, we focused on Caprin-1 as a key factor involved in the inhibition of SG formation in cells infected with JEV. To confirm the specific interaction of JEV core protein with Caprin-1, FLAG-JEV core protein and HA-Caprin-1 were coexpressed and immunoprecipitated with anti-HA or anti-FLAG antibody in the presence or absence of nuclease. FLAG-JEV core protein was coprecipitated with HA-Caprin-1 irrespective of nuclease treatment (Fig. 5C and D), suggesting that the interaction between JEV core protein and Caprin-1 is a protein-protein interaction. On the other hand, FLAG-DENV core protein was not coprecipitated with HA-Caprin-1 (Fig. 5E), indicating that the interaction with Caprin-1 was specific for JEV core protein. Next, the direct interaction be-

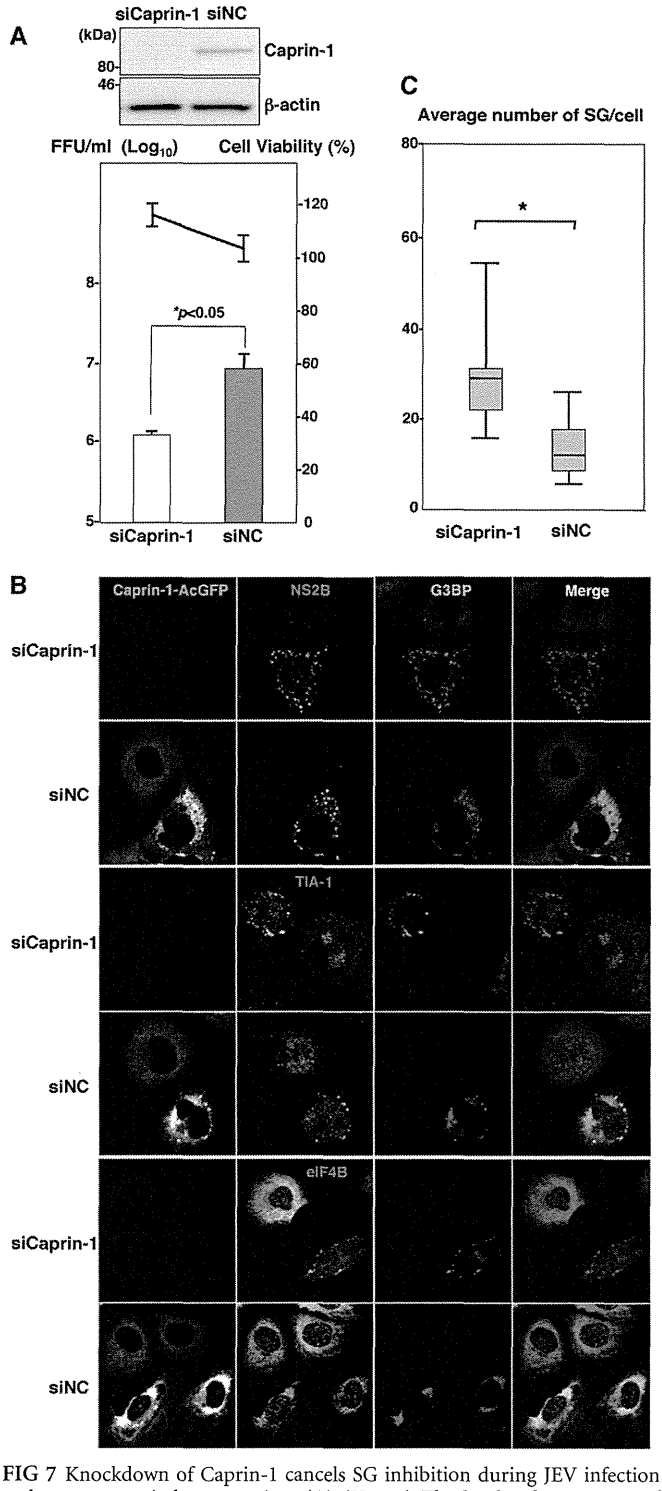

FIG 7 Knockdown of Caprin-1 cancels SG inhibition during JEV infection and suppresses viral propagation. (A) (Upper) The levels of expression of Caprin-1 in cells transfected with either siCaprin-1 or siNC was determined by immunoblotting using anti-Caprin-1 and anti-β-actin antibodies at 72 h posttransfection (top panel). At 48 h posttransfection with either siCaprin-1 or siNC, Huh7/Caprin-1-AcGFP cells were inoculated with JEV at an MOI of 0.5. At 24 h postinfection (72 h posttransfection), the infectious titers in the supernatants were determined by focus-forming assay in Vero cells (bottom panel, bar graph). Cell viability was determined at 72 h posttransfection and calculated as a percentage of the viability of cells treated with siNC (bottom panel, line graph). The results shown are from three independent assays, with the error bars representing the standard deviations. (B) At 48 h posttransfection with either siCaprin-1 or siNC, Huh7/Caprin-1-AcGFP cells were inoculated with JEV at an MOI of 0.5. The cellular localizations of SG-associated factors and JEV NS2B were determined at 24 h postinfection (72 h posttransfection) by immunofluorescence analysis with mouse anti-G3BP MAb and rabbit anti-NS2B PAb, rabbit anti-eIF4B PAb, or goat anti-TIA-1 PAb, followed by AF633-conjugated anti-mouse IgG and AF594-conjugated anti-rabbit IgG or AF594-conjugated anti-goat IgG, respectively. (C) Numbers of G3BP-positive foci in 30 cells prepared as described in panel B were counted. Lines, boxes, and error bars indicate the means, 25th to 75th percentiles, and 95th percentiles, respectively. The significance of differences between the means was determined by a Student's *t* test. *, $P < 0.01$.

tween JEV core protein and Caprin-1 was examined by a GST-pulldown assay using purified proteins expressed in bacteria. The His-tagged core protein was coprecipitated with GST-tagged Caprin-1, suggesting that JEV core protein directly interacts with Caprin-1 (Fig. 5F).

To further determine the cellular localization of Caprin-1 in JEV-infected cells, Caprin-1 fused with AcGFP (Caprin-1-AcGFP) was lentivirally expressed in Huh7 cells. The levels of expression and recruitment of Caprin-1-AcGFP into SGs were determined by immunoblotting and immunofluorescence analysis, respectively (Fig. 6A and B). In cells infected with JEV, Caprin-1-AcGFP was concentrated in the perinuclear region and colocalized with core protein and G3BP, while no colocalization of the proteins was observed in cells infected with DENV (Fig. 6C), suggesting that Caprin-1 directly interacts with JEV core protein in the perinuclear region of the infected cells.

Knockdown of Caprin-1 cancels SG inhibition during JEV infection and suppresses viral propagation. To assess the biological significance of the interaction of JEV core protein with Caprin-1 in JEV propagation, the expression of Caprin-1 was suppressed by using Caprin-1-specific siRNAs (siCaprin-1). Transfection of siCaprin-1 efficiently and specifically knocked down the expression of Caprin-1 with a slight increase of cell viability and decreased the production of infectious particles in the culture supernatants of cells infected with JEV, in comparison with those treated with a control siRNA (siNC) (Fig. 7A). Furthermore, immunofluorescence analyses revealed that knockdown of Caprin-1 increased the number of G3BP-positive granules colocalized with SG-associated factors, including TIA-1 and eIF4B, and inhibited the G3BP concentration in the perinuclear region (Fig. 7B and C). These results suggest that knockdown of Caprin-1 suppresses JEV propagation through the induction of SG formation.

Lys^{97} and Arg^{98} in the JEV core protein are crucial residues for the interaction with Caprin-1. To determine amino acid residues of the core protein that are required for the interaction with Caprin-1, we constructed a putative model based on the structural information of the DENV core protein previously resolved by nuclear magnetic resonance (NMR) (27), as shown in Fig. 8A. Based on this model, we selected hydrophobic amino acids, which were located on the solvent-exposed side in the α1 and α4 helices, as amino acid residues responsible for the binding to host proteins. Amino acid substitutions in each of the α-helices shown in Fig. 8B were designed in the context of FLAG-Core (Mα1 and Mα4), and the interaction of FLAG-Core mutants with Caprin-1 was examined by immunoprecipitation analysis. WT and Mα1, but not Mα4, core proteins were immunoprecipitated with Caprin-1 (Fig. 8B). To determine the amino acids responsible for interaction with Caprin-1, further alanine substitutions were introduced in the α4 helix, and the interaction was examined by immunopre-

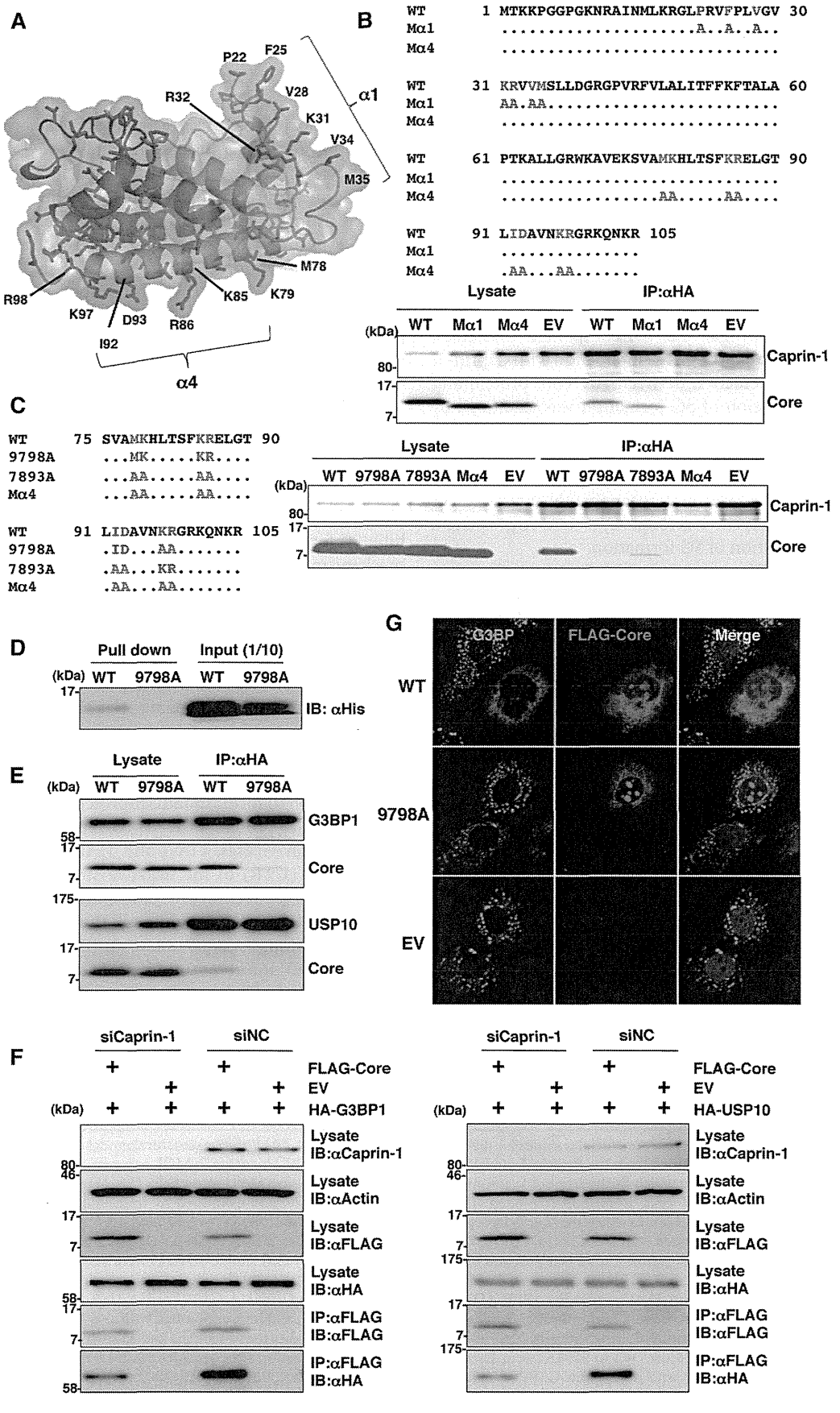

cipitation assay. As shown in Fig. 8C, double replacing both Lys^{97} and Arg^{98} with Ala (9798A) completely abrogated the interaction with Caprin-1. The importance of these two amino acids in the interaction with Caprin-1 was also confirmed by GST pulldown assay (Fig. 8D). These results indicate that Lys^{97} and Arg^{98} in the JEV core protein are crucial for the interaction with Caprin-1. Since G3BP has been reported to be one of the key molecules for SG formation and interacts with several SG component molecules including Caprin-1 and USP10 (28, 29), interactions of the core protein with SG components were examined by immunoprecipitation assay. The wild-type but not mutant 9798A core protein was associated with G3BP1 and USP10 (Fig. 8E). In addition, the knockdown of Caprin-1 weakened the interactions of core protein with G3BP1 or USP10 (Fig. 8F). These findings indicate that JEV core protein associates with several SG component molecules, such as G3BP1 and USP10, through the interaction with Caprin-1. Next, the role of the interaction between JEV core protein and Caprin-1 in the suppression of SG formation was examined by immunofluorescence analysis. Although the expression of the wild-type JEV core protein suppressed the SG formation induced by sodium arsenite treatment, as shown above, expression of the 9798A mutant did not (Fig. 8G), suggesting that the interaction of JEV core protein with Caprin-1 through Lys^{97} and Arg^{98} plays a crucial role in the inhibition of SG formation.

Interaction of the JEV core protein with Caprin-1 plays crucial roles not only in viral propagation *in vitro* but also in the pathogenesis in mice through the suppression of SG formation. To further examine the biological significance of the interaction between the JEV core protein and Caprin-1 in viral replication, we generated a mutant infectious cDNA clone (pMWJEAT/9798AA) of JEV encoding a mutant core protein deficient in the binding to Caprin-1 based on pMWJEAT. First, the cellular localization of the core protein in the 9798A mutant JEV-infected cells was examined by immunofluorescence analysis. The 9798A mutant core protein, as well as the wild-type core protein, was localized in the nucleus and the perinuclear region (Fig. 9A). However, the 9798A mutant core protein was not colocalized with Caprin-1, in contrast to the wild-type core protein. The sizes of infectious foci in Vero cells infected with the 9798A mutant were significantly smaller than those infected with the wild-type JEV (Fig. 9B). Furthermore, the infectious titers in C6/36 and Vero cells infected with the 9798A mutant were 6.1- and 12.6-fold lower than those infected with wild-type JEV at 48 h postinfection, respectively (Fig. 9C), suggesting that interaction of the JEV core protein with Caprin-1 plays crucial roles in the propagation of JEV in both insect and mammalian cells. Cells infected with the 9798A mutant induced SGs containing both G3BP and Caprin-1, in contrast to the accumulation of G3BP in the perinuclear region observed in those infected with the wild-type JEV (Fig. 9D). The numbers of foci in cells infected with the 9798A mutant were higher than those in cells infected with the wild-type JEV (Fig. 9E), indicating that the interaction of the JEV core protein with Caprin-1 is crucial for the suppression of SG formation. Finally, we examined the biological relevance of the interaction of JEV core protein with Caprin-1 in viral replication *in vivo*. Infectious particles were recovered from the cerebrums of ICR mice inoculated with wild-type JEV but not from those inoculated with the 9798A mutant (Fig. 9F). In addition, all 10 mice had died by 12 days postinoculation with the wild-type JEV, while only 1 mouse had died at day 10 postinoculation with the 9798A mutant (Fig. 9G). Collectively, these results suggest that the interaction of JEV core protein with Caprin-1 plays crucial roles not only in viral replication *in vitro* but also in pathogenesis in mice through the suppression of SG formation.

DISCUSSION

Viruses are obligatory intracellular parasites, and their life cycles rely on host cellular functions. Many viruses have evolved to inhibit SG formation and thereby evade the host translation shutoff mechanism and facilitate viral replication (6, 30), while some viruses co-opt molecules regulating SG formation for viral replication (11, 31). The vaccinia virus subverts SG components to generate aggregates containing G3BP, Caprin-1, eIF4G, eIF4E, and mRNA of the virus, but not of the host, in order to stimulate viral translation (11). Replication, translation, and assembly of transmissible gastroenteritis coronavirus, a member of the *Coronaviridae* family, are regulated by the interaction of polypyrimidine tract-binding protein and TIA-1 with viral RNA (31). HIV-1 utilizes Staufen1, which is a principal component of SG, in the viral RNA selection to form ribonucleoproteins (RNPs) through interaction with Gag protein, instead of SG translation silencing (8). In the case of flaviviruses, TIA-1 and TIAR bind to the 3′ untranslated region (UTR) of the negative-stranded RNA of WNV to facilitate viral replication (16), and G3BP1, Caprin-1, and USP10 interact with DENV RNA, although the biological significance of these interactions remains unknown (26). In this study, we have shown that JEV infection suppresses SG formation by the recruitment of several effector molecules promoting SG assembly, including G3BP and USP10, to the perinuclear region through the interaction of JEV core protein with Caprin-1. Furthermore, a mutant JEV carrying a core protein incapable of binding to

FIG 8 Lys^{97} and Arg^{98} in the JEV core protein are crucial residues for the interaction with Caprin-1. (A) Putative structural model of the core protein homodimer of JEV deduced from that of DENV obtained from the Protein Data Bank (accession number 1R6R) by using PyMOL software. The two α helices (α1 and α4) are indicated. (B) FLAG-Core mutants in which the hydrophobic amino acid residues in the α1 helix (Mα1) or α4 helix (Mα4) were replaced with alanine were coexpressed with HA-Caprin-1 in 293T cells, immunoprecipitated (IP) with anti-HA antibody, and examined by immunoblotting (IB) with anti-HA or anti-FLAG antibody. (C) FLAG-Core mutants in which the Met^{78}, Lys^{79}, Lys^{85}, Arg^{86}, Ile^{92}, and Asp^{93} (7893A) or Lys^{97} and Arg^{98} (9798A) in the α4 helix domain were replaced with alanine were coexpressed with HA-Caprin-1 in 293T cells and examined as described in panel B. (D) The His-tagged JEV core protein (WT or 9798A) was incubated with GST-fused Caprin-1 for 2 h at 4°C, and the precipitates obtained by GST pulldown assay were subjected to immunoblotting with anti-His antibody. (E) FLAG-Core (WT or 9798A) was coexpressed with HA-G3BP1 or HA-USP10 in 293T cells, immunoprecipitated with anti-HA antibody, and immunoblotted with anti-HA and anti-FLAG antibodies. (F) FLAG-JEV Core was coexpressed with HA-G3BP1 or HA-USP10 in 293T cells transfected with either siCaprin-1 or siNC at 72 h posttransfection, immunoprecipitated with anti-FLAG antibody, and immunoblotted with anti-HA and anti-FLAG antibodies. The cell lysates were also subjected to immunoblotting with anti-Caprin-1 and anti-β-actin antibodies to evaluate the knockdown efficiency of Caprin-1. (G) The cellular localizations of G3BP and FLAG-Core (WT or 9798A) were determined at 24 h posttransfection after treatment with 1.0 mM sodium arsenite for 30 min at 37°C by immunofluorescence analysis with mouse anti-G3BP MAb and rabbit anti-FLAG PAb, followed by AF488-conjugated anti-mouse IgG and AF594-conjugated anti-rabbit IgG, respectively. Cell nuclei were stained with DAPI (blue).

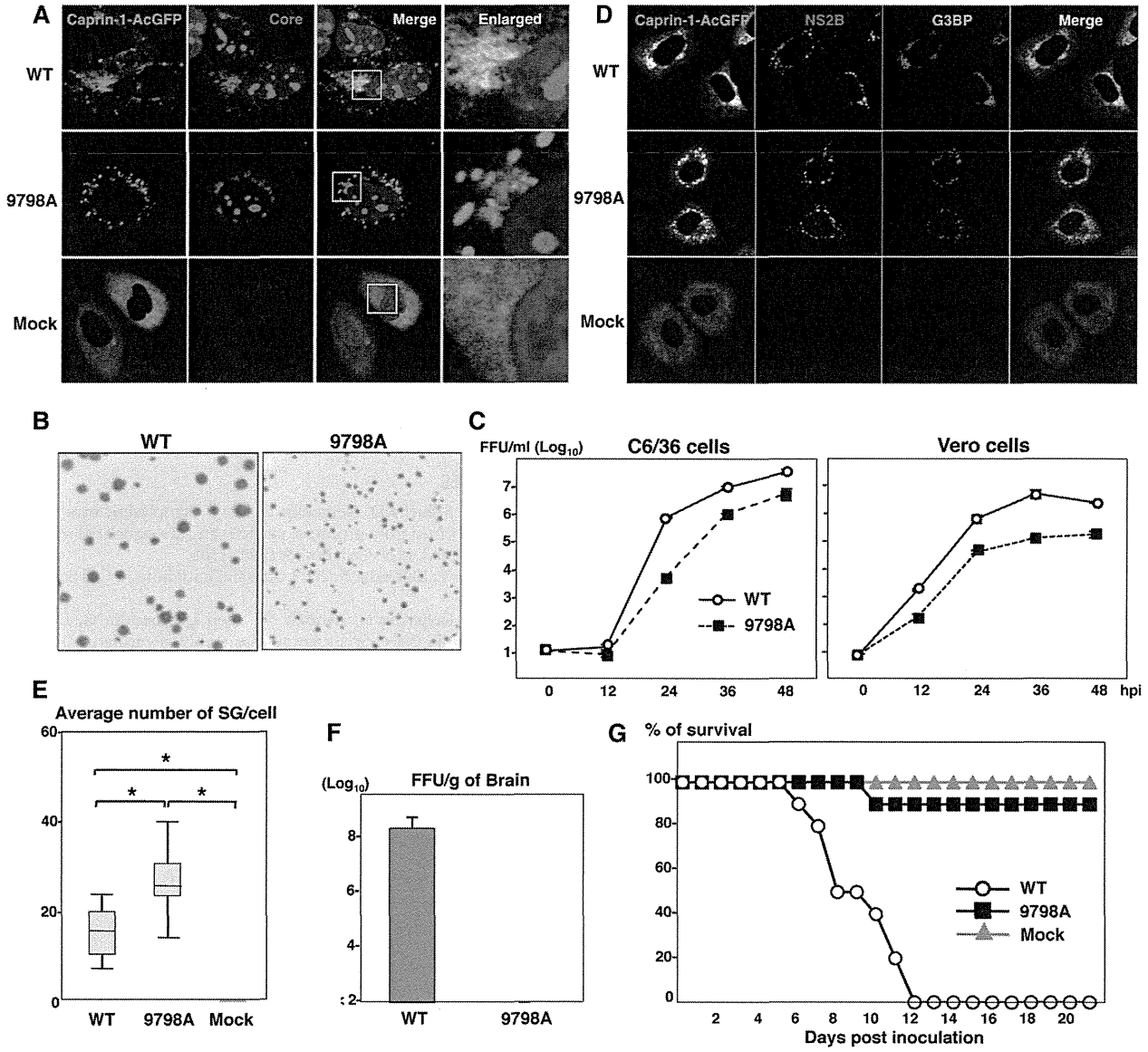

FIG 9 Interaction of JEV core protein with Caprin-1 plays crucial roles not only in viral replication *in vitro* but also in pathogenesis in mice through the suppression of SG formation. (A) Huh7/Caprin-1-AcGFP cells were infected with JEV (WT or 9798A mutant) at an MOI of 1.0, and the cellular localizations of Caprin-1-AcGFP and JEV core protein were determined at 24 h postinfection by immunofluorescence analysis with rabbit anti-core PAb and AF594-conjugated anti-rabbit IgG. Cell nuclei were stained with DAPI (blue). (B) Focus formation of JEV (WT or 9798A mutant) in Vero cells incubated in methylcellulose overlay medium at 48 h postinfection. The infectious foci were immunostained as described previously (20). (C) Growth kinetics of JEV (WT or 9798A mutant) in C6/36 and Vero cells infected at an MOI of 0.1. Infectious titers in the culture supernatants harvested at the indicated times were determined by focus-forming assays in Vero cells. Means of three experiments are indicated. (D) Huh7/Caprin-1-AcGFP cells were infected with either WT or 9798A at an MOI of 0.5, and cellular localizations of Caprin-1-AcGFP, G3BP (blue), and JEV NS2B (red) were determined at 24 h postinfection by immunofluorescence analysis with mouse anti-G3BP MAb and rabbit anti-NS2B PAb, followed by AF633-conjugated anti-mouse IgG and AF594-conjugated anti-rabbit IgG, respectively. (E) Numbers >of G3BP-positive foci in 30 cells prepared as described in panel D were counted. Lines, boxes, and error bars indicate the means, 25th to 75th percentiles, and 95th percentiles, respectively. The significance of differences between the means was determined by Student's *t* test. *, $P < 0.01$. (F) Infectious titers in the cerebrums of mice at 7 days postintraperitoneal inoculation with 5×10^4 FFU/100 μl of either WT or 9798A virus were determined in Vero cells. The means of titers in the homogenates of the cerebrums from three mice are indicated. The detection limit is 10^2 FFU/g of cerebrum. (G) Percentages of surviving mice ($n = 10$) after intraperitoneal inoculation with 5×10^4 FFU of either WT or 9798A virus. Mock, inoculation with DMEM.

Caprin-1 exhibited reduced replication *in vitro* and attenuated pathogenicity in mice.

G3BP is one of the key molecules involved in the SG aggregation process and self-oligomerizes in a phosphorylation-dependent manner to sequester mRNA in SGs (4). Therefore, G3BP knocked down cells (6) and G3BP knockout mouse embryonic fibroblast cells are deficient in the SG formation. In addition, G3BP sequestration inhibits SG formation in response to arsenite treatment (32). Caprin-1, known as RNA granule protein 105 or p137 (33), also participates in SG formation through phosphorylation of eIF2α (28) and is ubiquitously expressed in the cytoplasm. Caprin-1 regulates the transport and translation of mRNAs

of proteins involved in the synaptic plasticity in neurons (34) and cellular proliferation and migration in multiple cell types (28) through an interaction with G3BP. USP10, another SG-associated molecule, also interacts with G3BP and forms the G3BP/USP10 complex (29), suggesting that several SG-associated RBPs participate in the formation of a protein-protein network. In this study, the JEV core protein was shown to directly interact with Caprin-1, to sequester several key molecule complexes involved in SG formation to the perinuclear region in cells infected with JEV, and to facilitate viral propagation through the suppression of SG formation.

Flaviviruses replicate at a relatively low rate in comparison with most of the other positive-stranded RNA viruses, and thus rapid shutdown of host cellular protein synthesis would be deleterious for the viral life cycle. In cells infected with JEV, several SG components were colocalized with the core protein in the perinuclear region, while in those infected with WNV or DENV, SG components were accumulated in a replication complex composed of viral RNA and nonstructural proteins. In addition, the phosphorylation of eIF2α induced by arsenite was completely canceled by the infection with WNV or DENV, whereas the suppression of the phosphorylation was limited in JEV infection (15). Incorporation of the nascent viral RNA into the membranous structure induced by viral nonstructural proteins prevents PKR activation and inhibits SG formation in cells infected with WNV (17). In cells infected with hepatitis C virus (HCV), which belongs to the genus *Hepacivirus* in the family *Flaviviridae*, induction of SG formation was observed in the early stage of infection, in contrast to the inhibition of the arsenite-induced SG formation in the late stage (35). Several SG components, such as G3BP1, PABP1, and ataxin-2, were colocalized with HCV core protein around lipid droplets (35), and G3BP1 was also associated with the NS5B protein and the 5′ terminus of the minus-strand viral RNA (36) to mediate efficient viral replication. Collectively, these data suggest that flaviviruses have evolved to regulate cellular processes involved in SG formation through various strategies.

PKR is one of the interferon-stimulated genes and plays a crucial role in antiviral defense through phosphorylation of eIF2α, which leads to host translational shutoff (37, 38). In the early stage of flavivirus infection, both positive- and negative-stranded RNAs transcribe at low levels, while genomic RNA predominantly synthesizes in the late stage of infection (39). It was shown that activation of PKR was suppressed (40) or only induced in the late stage of WNV infection (41) and impaired by the expression of HCV NS5A (42–44). Very recently, JEV NS2A was shown to suppress PKR activation through inhibition of dimerization of PKR in the early stage but not in the late stage of infection (45). In this study, we have shown that JEV core protein interacts with Caprin-1 and inhibits SG formation downstream of the phosphorylation of eIF2α in the late stage of infection, suggesting that JEV has evolved to escape from host antiviral responses in the multiple stages of viral replication by using structural and nonstructural proteins.

The flavivirus core protein is a multifunctional protein involved in many aspects of the viral life cycle. In addition to the formation of viral nucleocapsid through the interaction with viral RNA (as a structural protein) (46), flavivirus core proteins interact with various host factors, such as B23 (47), Jab1 (48), hnRNP K (49), and hnRNP A2 (23), and regulate viral replication and/or modify the host cell environment (as a nonstructural protein). Although further investigations are needed to clarify the precise mechanisms underlying the circumvention of SG formation through the interaction of JEV core protein with Caprin-1, leading to efficient propagation *in vitro* and pathogenicity in mice, these findings could help not only to provide new insight into strategies by which viruses escape host stress responses but also to develop novel antiviral agents for flavivirus infection.

ACKNOWLEDGMENTS

We thank M. Tomiyama for secretarial assistance. We also thank K. Saito and T. Wakita for technical advice and the infectious clone of JEV, respectively.

This work was supported in part by grants-in-aid from the Ministry of Health, Labor, and Welfare, the Ministry of Education, Culture, Sports, Science, and Technology, and the Osaka University Global Center of Excellence Program. H. Katoh is a research fellow of the Japanese Society for the Promotion of Science.

REFERENCES

1. **Nover L, Scharf KD, Neumann D.** 1989. Cytoplasmic heat shock granules are formed from precursor particles and are associated with a specific set of mRNAs. Mol. Cell. Biol. **9**:1298–1308.
2. **Anderson P, Kedersha N.** 2002. Stressful initiations. J. Cell Sci. **115**:3227–3234.
3. **Gilks N, Kedersha N, Ayodele M, Shen L, Stoecklin G, Dember LM, Anderson P.** 2004. Stress granule assembly is mediated by prion-like aggregation of TIA-1. Mol. Biol. Cell **15**:5383–5398.
4. **Tourriere H, Chebli K, Zekri L, Courselaud B, Blanchard JM, Bertrand E, Tazi J.** 2003. The RasGAP-associated endoribonuclease G3BP assembles stress granules. J. Cell Biol. **160**:823–831.
5. **Kedersha N, Cho MR, Li W, Yacono PW, Chen S, Gilks N, Golan DE, Anderson P.** 2000. Dynamic shuttling of TIA-1 accompanies the recruitment of mRNA to mammalian stress granules. J. Cell Biol. **151**:1257–1268.
6. **White JP, Cardenas AM, Marissen WE, Lloyd RE.** 2007. Inhibition of cytoplasmic mRNA stress granule formation by a viral proteinase. Cell Host Microbe **2**:295–305.
7. **Khaperskyy DA, Hatchette TF, McCormick C.** 2012. Influenza A virus inhibits cytoplasmic stress granule formation. FASEB J. **26**:1629–1639.
8. **Abrahamyan LG, Chatel-Chaix L, Ajamian L, Milev MP, Monette A, Clement JF, Song R, Lehmann M, DesGroseillers L, Laughrea M, Boccaccio G, Mouland AJ.** 2010. Novel Staufen1 ribonucleoproteins prevent formation of stress granules but favour encapsidation of HIV-1 genomic RNA. J. Cell Sci. **123**:369–383.
9. **McInerney GM, Kedersha NL, Kaufman RJ, Anderson P, Liljestrom P.** 2005. Importance of eIF2α phosphorylation and stress granule assembly in alphavirus translation regulation. Mol. Biol. Cell **16**:3753–3763.
10. **Smith JA, Schmechel SC, Raghavan A, Abelson M, Reilly C, Katze MG, Kaufman RJ, Bohjanen PR, Schiff LA.** 2006. Reovirus induces and benefits from an integrated cellular stress response. J. Virol. **80**:2019–2033.
11. **Katsafanas GC, Moss B.** 2007. Colocalization of transcription and translation within cytoplasmic poxvirus factories coordinates viral expression and subjugates host functions. Cell Host Microbe **2**:221–228.
12. **Misra UK, Kalita J.** 2010. Overview: Japanese encephalitis. Prog. Neurobiol. **91**:108–120.
13. **Sumiyoshi H, Mori C, Fuke I, Morita K, Kuhara S, Kondou J, Kikuchi Y, Nagamatu H, Igarashi A.** 1987. Complete nucleotide sequence of the Japanese encephalitis virus genome RNA. Virology **161**:497–510.
14. **Murray CL, Jones CT, Rice CM.** 2008. Architects of assembly: roles of *Flaviviridae* non-structural proteins in virion morphogenesis. Nat. Rev. Microbiol. **6**:699–708.
15. **Emara MM, Brinton MA.** 2007. Interaction of TIA-1/TIAR with West Nile and dengue virus products in infected cells interferes with stress granule formation and processing body assembly. Proc. Natl. Acad. Sci. U. S. A. **104**:9041–9046.
16. **Li W, Li Y, Kedersha N, Anderson P, Emara M, Swiderek KM, Moreno GT, Brinton MA.** 2002. Cell proteins TIA-1 and TIAR interact with the 3′ stem-loop of the West Nile virus complementary minus-strand RNA and facilitate virus replication. J. Virol. **76**:11989–12000.
17. **Courtney SC, Scherbik SV, Stockman BM, Brinton MA.** 2012. West Nile

virus infections suppress early viral RNA synthesis and avoid inducing the cell stress granule response. J. Virol. 86:3647–3657.
18. Kambara H, Tani H, Mori Y, Abe T, Katoh H, Fukuhara T, Taguwa S, Moriishi K, Matsuura Y. 2011. Involvement of cyclophilin B in the replication of Japanese encephalitis virus. Virology 412:211–219.
19. Mori Y, Yamashita T, Tanaka Y, Tsuda Y, Abe T, Moriishi K, Matsuura Y. 2007. Processing of capsid protein by cathepsin L plays a crucial role in replication of Japanese encephalitis virus in neural and macrophage cells. J. Virol. 81:8477–8487.
20. Mori Y, Okabayashi T, Yamashita T, Zhao Z, Wakita T, Yasui K, Hasebe F, Tadano M, Konishi E, Moriishi K, Matsuura Y. 2005. Nuclear localization of Japanese encephalitis virus core protein enhances viral replication. J. Virol. 79:3448–3458.
21. Kambara H, Fukuhara T, Shiokawa M, Ono C, Ohara Y, Kamitani W, Matsuura Y. 2012. Establishment of a novel permissive cell line for the propagation of hepatitis C virus by expression of microRNA miR122. J. Virol. 86:1382–1393.
22. Zhao Z, Date T, Li Y, Kato T, Miyamoto M, Yasui K, Wakita T. 2005. Characterization of the E-138 (Glu/Lys) mutation in Japanese encephalitis virus by using a stable, full-length, infectious cDNA clone. J. Gen. Virol. 86:2209–2220.
23. Katoh H, Mori Y, Kambara H, Abe T, Fukuhara T, Morita E, Moriishi K, Kamitani W, Matsuura Y. 2011. Heterogeneous nuclear ribonucleoprotein A2 participates in the replication of Japanese encephalitis virus through an interaction with viral proteins and RNA. J. Virol. 85:10976–10988.
24. Hamamoto I, Nishimura Y, Okamoto T, Aizaki H, Liu M, Mori Y, Abe T, Suzuki T, Lai MM, Miyamura T, Moriishi K, Matsuura Y. 2005. Human VAP-B is involved in hepatitis C virus replication through interaction with NS5A and NS5B. J. Virol. 79:13473–13482.
25. Jones CT, Ma L, Burgner JW, Groesch TD, Post CB, Kuhn RJ. 2003. Flavivirus capsid is a dimeric alpha-helical protein. J. Virol. 77:7143–7149.
26. Ward AM, Bidet K, Yinglin A, Ler SG, Hogue K, Blackstock W, Gunaratne J, Garcia-Blanco MA. 2011. Quantitative mass spectrometry of DENV-2 RNA-interacting proteins reveals that the DEAD-box RNA helicase DDX6 binds the DB1 and DB2 3′ UTR structures. RNA Biol. 8:1173–1186.
27. Ma L, Jones CT, Groesch TD, Kuhn RJ, Post CB. 2004. Solution structure of dengue virus capsid protein reveals another fold. Proc. Natl. Acad. Sci. U. S. A. 101:3414–3419.
28. Solomon S, Xu Y, Wang B, David MD, Schubert P, Kennedy D, Schrader JW. 2007. Distinct structural features of Caprin-1 mediate its interaction with G3BP-1 and its induction of phosphorylation of eukaryotic translation initiation factor 2α, entry to cytoplasmic stress granules, and selective interaction with a subset of mRNAs. Mol. Cell. Biol. 27:2324–2342.
29. Soncini C, Berdo I, Draetta G. 2001. Ras-GAP SH3 domain binding protein (G3BP) is a modulator of USP10, a novel human ubiquitin specific protease. Oncogene 20:3869–3879.
30. Montero H, Rojas M, Arias CF, Lopez S. 2008. Rotavirus infection induces the phosphorylation of eIF2α but prevents the formation of stress granules. J. Virol. 82:1496–1504.
31. Sola I, Galan C, Mateos-Gomez PA, Palacio L, Zuniga S, Cruz JL, Almazan F, Enjuanes L. 2011. The polypyrimidine tract-binding protein affects coronavirus RNA accumulation levels and relocalizes viral RNAs to novel cytoplasmic domains different from replication-transcription sites. J. Virol. 85:5136–5149.
32. Hinton SD, Myers MP, Roggero VR, Allison LA, Tonks NK. 2010. The pseudophosphatase MK-STYX interacts with G3BP and decreases stress granule formation. Biochem. J. 427:349–357.
33. Grill B, Wilson GM, Zhang KX, Wang B, Doyonnas R, Quadroni M, Schrader JW. 2004. Activation/division of lymphocytes results in increased levels of cytoplasmic activation/proliferation-associated protein-1: prototype of a new family of proteins. J. Immunol. 172:2389–2400.
34. Shiina N, Shinkura K, Tokunaga M. 2005. A novel RNA-binding protein in neuronal RNA granules: regulatory machinery for local translation. J. Neurosci. 25:4420–4434.
35. Ariumi Y, Kuroki M, Kushima Y, Osugi K, Hijikata M, Maki M, Ikeda M, Kato N. 2011. Hepatitis C virus hijacks P-body and stress granule components around lipid droplets. J. Virol. 85:6882–6892.
36. Yi Z, Pan T, Wu X, Song W, Wang S, Xu Y, Rice CM, Macdonald MR, Yuan Z. 2011. Hepatitis C virus co-opts Ras-GTPase-activating protein-binding protein 1 for its genome replication. J. Virol. 85:6996–7004.
37. Gale M, Jr, Katze MG. 1998. Molecular mechanisms of interferon resistance mediated by viral-directed inhibition of PKR, the interferon-induced protein kinase. Pharmacol. Ther. 78:29–46.
38. Pindel A, Sadler A. 2011. The role of protein kinase R in the interferon response. J. Interferon Cytokine Res. 31:59–70.
39. Chu PW, Westaway EG. 1985. Replication strategy of Kunjin virus: evidence for recycling role of replicative form RNA as template in semiconservative and asymmetric replication. Virology 140:68–79.
40. Elbahesh H, Scherbik SV, Brinton MA. 2011. West Nile virus infection does not induce PKR activation in rodent cells. Virology 421:51–60.
41. Samuel MA, Whitby K, Keller BC, Marri A, Barchet W, Williams BR, Silverman RH, Gale M, Jr, Diamond MS. 2006. PKR and RNase L contribute to protection against lethal West Nile Virus infection by controlling early viral spread in the periphery and replication in neurons. J. Virol. 80:7009–7019.
42. Gale M, Jr, Blakely CM, Kwieciszewski B, Tan SL, Dossett M, Tang NM, Korth MJ, Polyak SJ, Gretch DR, Katze MG. 1998. Control of PKR protein kinase by hepatitis C virus nonstructural 5A protein: molecular mechanisms of kinase regulation. Mol. Cell. Biol. 18:5208–5218.
43. Gale MJ, Jr, Korth MJ, Tang NM, Tan SL, Hopkins DA, Dever TE, Polyak SJ, Gretch DR, Katze MG. 1997. Evidence that hepatitis C virus resistance to interferon is mediated through repression of the PKR protein kinase by the nonstructural 5A protein. Virology 230:217–227.
44. He Y, Tan SL, Tareen SU, Vijaysri S, Langland JO, Jacobs BL, Katze MG. 2001. Regulation of mRNA translation and cellular signaling by hepatitis C virus nonstructural protein NS5A. J. Virol. 75:5090–5098.
45. Tu YC, Yu CY, Liang JJ, Lin E, Liao CL, Lin YL. 2012. Blocking dsRNA-activated protein kinase PKR by Japanese encephalitis virus nonstructural protein 2A. J. Virol. 86:10347–10358.
46. Khromykh AA, Westaway EG. 1996. RNA binding properties of core protein of the flavivirus Kunjin. Arch. Virol. 141:685–699.
47. Tsuda Y, Mori Y, Abe T, Yamashita T, Okamoto T, Ichimura T, Moriishi K, Matsuura Y. 2006. Nucleolar protein B23 interacts with Japanese encephalitis virus core protein and participates in viral replication. Microbiol. Immunol. 50:225–234.
48. Oh W, Yang MR, Lee EW, Park KM, Pyo S, Yang JS, Lee HW, Song J. 2006. Jab1 mediates cytoplasmic localization and degradation of West Nile virus capsid protein. J. Biol. Chem. 281:30166–30174.
49. Chang CJ, Luh HW, Wang SH, Lin HJ, Lee SC, Hu ST. 2001. The heterogeneous nuclear ribonucleoprotein K (hnRNP K) interacts with dengue virus core protein. DNA Cell Biol. 20:569–577.

Zinc-finger antiviral protein mediates retinoic acid inducible gene I–like receptor-independent antiviral response to murine leukemia virus

Hanna Lee[a,b], Jun Komano[c], Yasunori Saitoh[d], Shoji Yamaoka[d], Tatsuya Kozaki[a,b], Takuma Misawa[a,b], Michihiro Takahama[a,b], Takashi Satoh[a,b], Osamu Takeuchi[e], Naoki Yamamoto[f], Yoshiharu Matsuura[g], Tatsuya Saitoh[a,b,1], and Shizuo Akira[a,b,1]

[a]Laboratory of Host Defense, World Premier International Immunology Frontier Research Center, Osaka University, Osaka 565-0871, Japan; Departments of [b]Host Defense and [g]Molecular Virology, Research Institute for Microbial Diseases, Osaka University, Osaka 565-0871, Japan; [c]Department of Infectious Diseases, Osaka Prefectural Institute of Public Health, Osaka 537-0025, Japan; [d]Department of Molecular Virology, Graduate School of Medical and Dental Sciences, Tokyo Medical and Dental University, Tokyo 113-8519, Japan; [e]Laboratory of Infection and Prevention, Institute for Virus Research, Kyoto University, Kyoto 606-8507, Japan; and [f]Department of Microbiology, Yong Loo Lin School of Medicine, National University of Singapore, Singapore 117599

Contributed by Shizuo Akira, June 5, 2013 (sent for review May 14, 2013)

When host cells are infected by an RNA virus, pattern-recognition receptors (PRRs) recognize the viral RNA and induce the antiviral innate immunity. Toll-like receptor 7 (TLR7) detects the genomic RNA of incoming murine leukemia virus (MLV) in endosomes and mediates the antiviral response. However, the RNA-sensing PRR that recognizes the MLV in the cytosol is not fully understood. Here, we definitively demonstrate that zinc-finger antiviral protein (ZAP) acts as a cytosolic RNA sensor, inducing the degradation of the MLV transcripts by the exosome, an RNA degradation system, on RNA granules. Although the retinoic acid inducible gene I (RIG-I)–like receptors (RLRs) RIG-I and melanoma differentiation-associated protein 5 detect various RNA viruses in the cytosol and induce the type I IFN-dependent antiviral response, RLR loss does not alter the replication efficiency of MLV. In sharp contrast, the loss of ZAP greatly enhances the replication efficiency of MLV. ZAP localizes to RNA granules, where the processing-body and stress-granule proteins assemble. ZAP induces the recruitment of the MLV transcripts and exosome components to the RNA granules. The CCCH-type zinc-finger domains of ZAP, which are RNA-binding motifs, mediate its localization to RNA granules and MLV transcripts degradation by the exosome. Although ZAP was known as a regulator of RIG-I signaling in a human cell line, ZAP deficiency does not affect the RIG-I–dependent production of type I IFN in mouse cells. Thus, ZAP is a unique member of the cytosolic RNA-sensing PRR family that targets and eliminates intracellular RNA viruses independently of TLR and RLR family members.

host defense | retrovirus | ZC3HAV1

Innate immunity is induced after the recognition of viral RNAs by pattern-recognition receptors (PRRs) and is the first line of the host defenses against a variety of RNA viruses (1, 2). Among the PRRs, the Toll-like receptor (TLR) and retinoic acid-inducible gene I (RIG-I)-like receptor (RLR) families play major roles in the recognition of viral RNAs. The RLR's RIG-I [also called DEAD (Asp-Glu-Ala-Asp) box polypeptide 58 (DDX58)] and melanoma differentiation-associated protein 5 [MDA5, also called interferon induced with helicase C domain 1 (IFIH1)] are RNA helicases that sense the ds form of viral RNAs in the cytosol (3, 4). After sensing dsRNA, the RLRs trigger a signaling pathway that activates interferon (IFN) regulatory factor 3 (IRF3) and IRF7, transcription factors that induce IFN stimulation-responsive, element-dependent transcription (5, 6). This results in the production of type I IFN and the expression of IFN-inducible antiviral proteins. The sensing of viral RNAs by TLR family members also induces the IRF3- and IRF7-dependent type I IFN response (1, 2). In epithelial cells, TLR3, a sensor of dsRNA, detects the incoming RNA virus genomes in endosomes and induces the activation of IRF3, leading to the production of type I IFN (7, 8). In plasmacytoid dendritic cells, TLR7, a sensor of single-stranded (ss) RNA, detects incoming RNA virus genomes in endo-lysosomes and triggers the activation of IRF7, leading to the robust production of type I IFN (9–13). Thus, TLRs and RLRs play major roles in the establishment of an antiviral state by mediating the production of type I IFN.

Murine leukemia virus (MLV), a retrovirus belonging to the gammaretroviral genus of the family *Retroviridae*, is a causative agent of cancer in murine hosts (14, 15). Although type I IFN is essential for the protection of hosts from lethal infection with a variety of RNA viruses, such as influenza A virus (IAV) and vesicular stomatitis virus (VSV), type I IFN is not essential for induction of the antiviral state against MLV (16–18). Therefore, a different type of innate immune system has been proposed to protect hosts from MLV infection. Although TLR7 has been shown to induce virus-neutralizing immunity after MLV genomic RNA is detected in endosomes (16), the RNA sensor responsible for the elimination of MLV in the cytosol has not been fully understood. RLRs are candidate RNA sensors of intracellular MLV. RLRs might mediate the antiviral response to MLV after the viral RNA is detected, independently of type I IFN because RLRs stimulate not only IRF3/IRF7, but also other transcription factors, such as NF-κB and activator protein 1, which are responsible for the production of inflammatory cytokines and chemokines (19). Another candidate sensor is zinc-finger antiviral protein [ZAP, also called zinc finger CCCH-type, antiviral 1 (ZC3HAV1)]. ZAP was originally identified with an expression cloning method as one of the antiviral proteins directed against MLV (20). ZAP reduces the level of MLV transcripts in the cytosol to suppress MLV infection at the posttranscriptional stage, whereas ZAP does not inhibit the early stage of the MLV infection. ZAP recognizes the MLV transcripts via its CCCH-type zinc-finger domains and binds with RNA helicases and the components of the exosome (an RNA degradation system) to induce the degradation of the MLV transcripts (21–25). However, it is unclear whether endogenous ZAP is involved in the antiviral response to replication-competent MLV in primary cells. In the present study, we examined the roles of these two types of cytosolic RNA sensors and demonstrated the spatial regulation of the innate immune response directed against intracellular MLV.

Author contributions: T. Saitoh and S.A. designed research; H.L., J.K., Y.S., S.Y., T.K., T.M., M.T., T. Satoh, O.T., N.Y., and Y.M. performed research; and T. Saitoh wrote the paper.

The authors declare no conflict of interest.

[1]To whom correspondence may be addressed. E-mail: sakira@biken.osaka-u.ac.jp or tatsuya@biken.osaka-u.ac.jp.

This article contains supporting information online at www.pnas.org/lookup/suppl/doi:10.1073/pnas.1310604110/-/DCSupplemental.

Results

RLRs Do Not Regulate the Antiviral Response to MLV in Primary Mouse Embryonic Fibroblasts. We first examined the involvement of RLRs in the antiviral response to MLV in mouse embryonic fibroblasts (MEFs). The replication efficiency of MLV in *Ddx58*$^{-/-}$/*Ifih1*$^{-/-}$ MEFs was similar to that in *Ddx58*$^{+/+}$/*Ifih1*$^{+/+}$ MEFs (Fig. 1*A*). Furthermore, the replication efficiency of MLV in *Irf3*$^{-/-}$/*Irf7*$^{-/-}$ MEFs was similar to that in *Irf3*$^{+/-}$/*Irf7*$^{+/-}$ MEFs (Fig. 1*B*). Consistent with this, the levels of *Ifnb1* and *chemokine (C-X-C motif) ligand 10* (*Cxcl10*) mRNAs did not change during MLV infection (Fig. 1 *C–F*). The RLR–IRF3/7 signaling axis is essential for the up-regulation of *Ifnb1* and *Cxcl10* mRNAs during VSV infection. R848, a ligand of TLR7, failed to stimulate MEFs isolated from C57BL/6 mice (Fig. S1), indicating that no RNA-sensing TLR family member recognizes MLV in the extracellular space of MEFs. Therefore, MLV evades the RLR and TLR systems and does not induce the type I IFN response in MEFs.

Endogenous ZAP Limits the Replication of MLV in Primary MEFs. We next investigated the role of ZAP, another cytosolic sensor of viral RNA, in the antiviral response to MLV. Previous studies have demonstrated that the ectopic expression of ZAP potently inhibits replication-incompetent MLV in the cytoplasm of various types of cell lines (20). Therefore, we generated *Zc3hav1*$^{-/-}$ mice to examine whether endogenous ZAP controls the replication of MLV in primary cells (Fig. S2). Detectable levels of ZAP protein were expressed in *Zc3hav1*$^{+/+}$ MEFs before and after MLV infection (Fig. S2*D*). Whereas ZAP deficiency did not alter the replication efficiency of VSV in MEFs (Fig. S3), ZAP deficiency greatly enhanced the replication efficiency of MLV (Fig. 2 *A* and *B*). These findings indicate that endogenous ZAP is responsible for the antiviral response to replication-competent MLV in primary mouse cells.

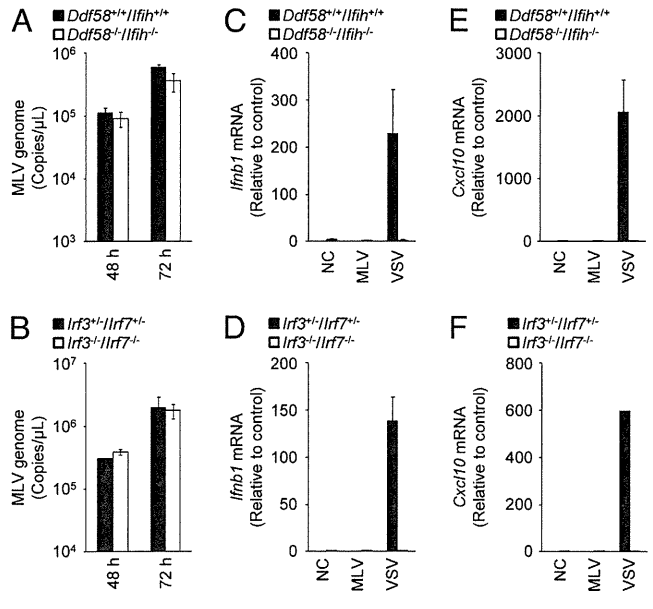

Fig. 1. RIG-I–like receptors are not essential for the antiviral response to MLV in primary MEFs. (*A* and *B*) *Ddx58*$^{+/+}$/*Ifih1*$^{+/+}$ and *Ddx5*$^{-/-}$/*Ifih1*$^{-/-}$ MEFs (*A*) or *Irf3*$^{+/-}$/*Irf7*$^{+/-}$ and *Irf*$^{-/-}$/*Irf7*$^{-/-}$ MEFs (*B*) were infected with MLV (2×10^{10} copies per μL) for 48 or 72 h. The copy numbers of the MLV genome in the culture supernatants were measured by quantitative RT-PCR. (*C–F*) *Ddx58*$^{+/+}$/*Ifih1*$^{+/+}$ and *Ddx58*$^{-/-}$/*Ifih1*$^{-/-}$ MEFs (*C* and *E*) or *Irf3*$^{+/-}$/*Irf7*$^{+/-}$ and *Irf3*$^{-/-}$/*Irf7*$^{-/-}$ MEFs (*D* and *F*) were infected with MLV (2×10^{10} copies per μL) or VSV [multiplicity of infection (MOI) = 1] for 12 h. The levels of *Ifnb1* (*C* and *D*) and *Cxcl10* (*E* and *F*) mRNAs were measured by quantitative RT-PCR. The results shown are means ± SD ($n = 3$).

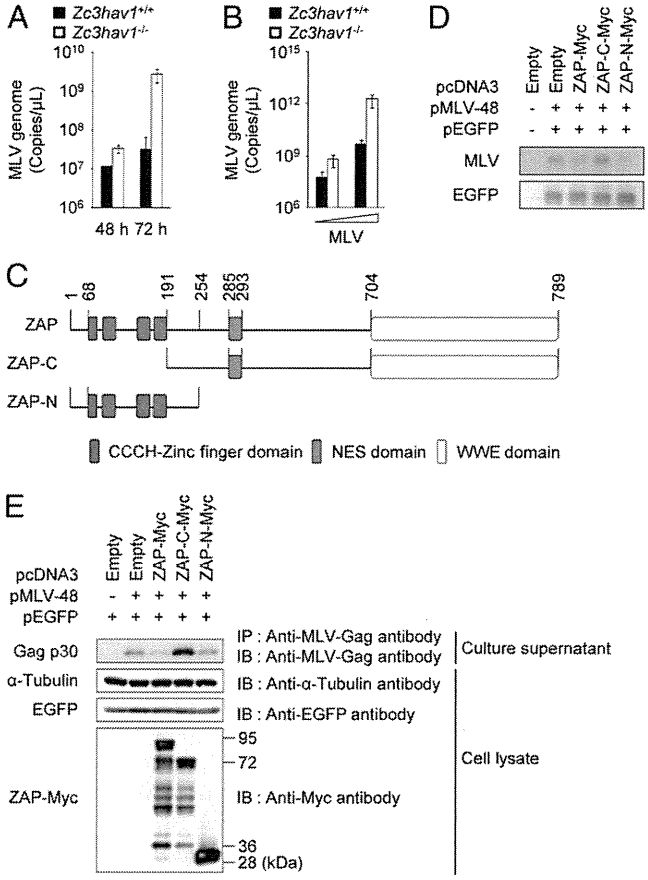

Fig. 2. ZAP inhibits MLV replication in primary MEFs. (*A*) *Zc3hav1*$^{+/+}$ and *Zc3hav1*$^{-/-}$ MEFs were infected with MLV (2×10^{10} copies per μL). Viral RNA was isolated at the indicated time points. The copy numbers of the MLV genome in the culture supernatants were measured by quantitative RT-PCR. (*B*) *Zc3hav1*$^{+/+}$ and *Zc3hav1*$^{-/-}$ MEFs were infected with increasing doses of MLV (2×10^{8} and 2×10^{9} copies per μL) for 96 h. The copy numbers of the MLV genome in the culture supernatants were measured by quantitative RT-PCR. (*C*) Domain architecture of ZAP. (*D* and *E*) 293T cells were transfected with pMLV-48 and pEGFP-N1 together with the indicated ZAP expression plasmids for 48 h. Cytoplasmic RNA was subjected to Northern blotting analysis of the indicated RNAs (*D*). The culture supernatants were subjected to immunoprecipitation coupled to immunoblotting to detect the indicated proteins (*E*). The results shown are means ± SD ($n = 3$). NES, nuclear export signal.

The CCCH-type zinc-finger domains of ZAP are known to recognize the MLV transcripts and to induce its degradation (21, 25). Consistent with this, the ectopic expression of the N-terminal portion of ZAP, which contains the CCCH-type zinc-finger domains, but not the ectopic expression of the C-terminal portion of ZAP, which lacks CCCH-type zinc-finger domains, reduced the level of MLV transcripts in the cytosol (Fig. 2 *C* and *D*). The ectopic expression of the CCCH-type zinc-finger domains of ZAP also suppressed the expression of the Gag protein of MLV (Fig. 2*E*). Therefore, the CCCH-type zinc-finger domains of ZAP are essential for its antiviral action against MLV.

CCCH-Type Zinc-Finger Domains of ZAP Mediate Its Localization to the RNA Granules. The involvement of ZAP in the antiviral response to MLV prompted us to determine the mechanism underlying the ZAP-dependent degradation of the MLV transcripts. Although a previous study showed that ZAP acts in the cytosol (20), it was still unclear where in the cytosol ZAP eliminates the MLV transcripts. Therefore, we examined whether ZAP localizes to a cytosolic compartment, such as in the processing bodies

(P-bodies) (26). When it was ectopically expressed, ZAP localized to cytoplasmic dot-like structures in a manner that was dependent on its CCCH-type zinc-finger domains (Fig. 3*A*). The ZAP-positive dot-like structures colocalized with marker proteins for P-bodies, such as DCP1 decapping enzyme homolog A (*Saccharomyces cerevisiae*; DCP1A) and DDX6 (Fig. 3*B*). ZAP induced the enlargement of the DCP1A- and DDX6-positive dot-like structures, suggesting that the ZAP-positive dot-like structures are not conventional P-bodies. ZAP also colocalized with marker proteins for stress granules, such as GTPase-activating protein (SH3 domain) binding protein 1 (G3BP1) and cytotoxic granule-associated RNA binding protein (TIA-1) (Fig. S4). Furthermore, the RNA helicase DEAH (Asp-Glu-Ala-His) box polypeptide 30 (DHX30), which binds to ZAP to facilitate its antiviral action against MLV (24), colocalized with ZAP to the DCP1A-positive dot-like structures (Fig. S5). By contrast, ZAP did not colocalize with mitochondrial preprotein translocases of the outer membrane 20 (TOM20), 70-kDa peroxisomal membrane protein (PMP70), early endosome antigen 1 (EEA1), or lysosomal-associated membrane protein 1 (LAMP1), marker proteins for the mitochondria, peroxisomes, endosomes, and lysosomes, respectively (Fig. 3*C*). These findings indicate that ZAP localizes to the RNA granules, where the marker proteins for P-bodies and stress granules assemble.

ZAP Recruits the MLV Transcripts and Exosome Components to RNA Granules. The localization of the MLV transcripts has been poorly understood. We used an improved RNA FISH method to visualize the subcellular localization of viral RNA and identified the cytosolic compartments in which ZAP acts on the MLV transcripts. The MLV transcripts mainly localize in the cytosol and colocalize with DCP1A-positive RNA granules at low frequency (Fig. 4). However, the ectopic expression of ZAP reduced the level of MLV transcripts in the cytosol and dramatically altered its localization from the cytosol to ZAP- and DCP1A-positive RNA granules (Fig. 4 and Fig. S6). Therefore, ZAP tethers the MLV transcripts and transfers it to the RNA granules.

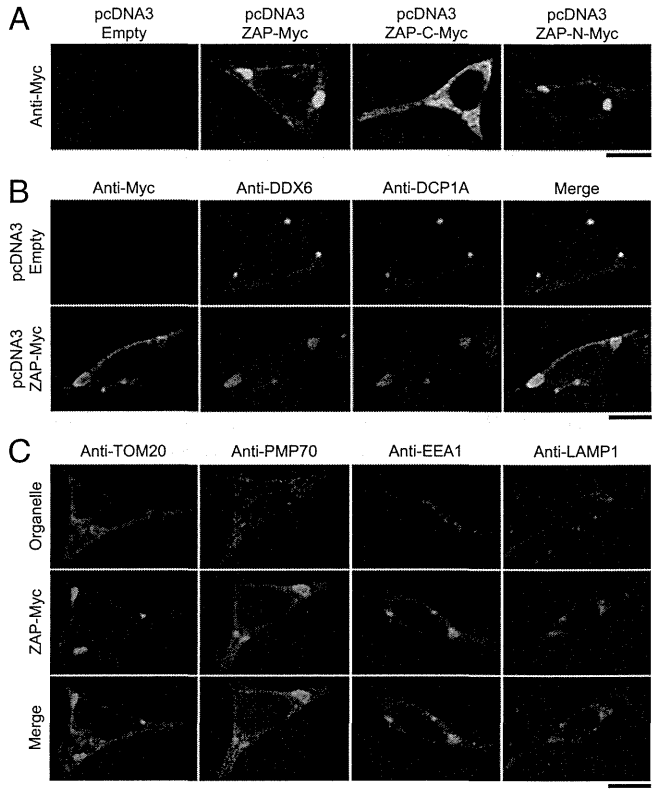

Fig. 3. ZAP localizes to DCP1A- and DDX6-positive RNA granules. (*A–C*) 293T cells were transfected with the indicated vectors for 48 h and then fixed. The samples were immunostained with the indicated antibodies and then observed by confocal laser scanning microscopy. The data are representative of three independent experiments. (Scale bars, 10 μm.)

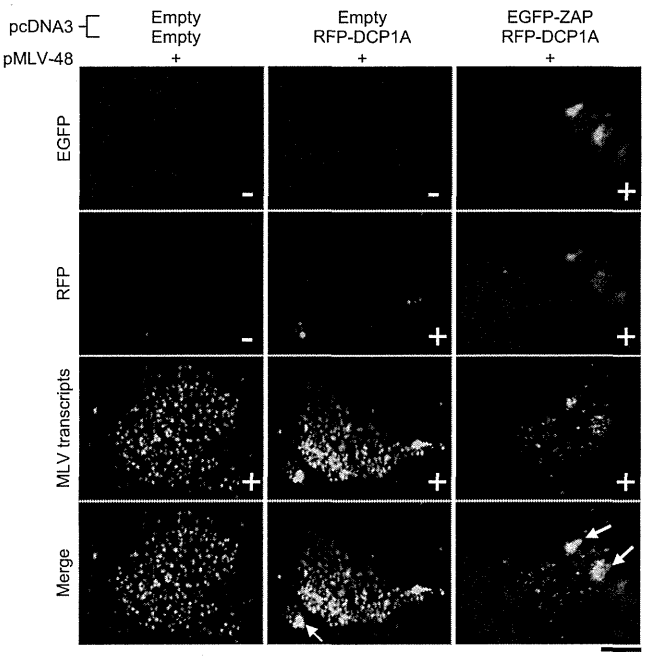

Fig. 4. ZAP recruits the MLV transcripts to RNA granules. 293T cells were transfected with the indicated plasmids for 48 h and then fixed. The samples were subjected to in situ hybridization analysis with a fluorescent probe for MLV transcripts and then observed by confocal laser scanning microscopy. (Scale bar, 10 μm.)

Because ZAP is not a ribonuclease, it requires the support of an RNA degradation system to destabilize the MLV transcripts. Consistent with this, previous studies have shown that exosome components and RNA helicases interact with ZAP to mediate the antiviral response to MLV (22–24). Therefore, we focused on the localization of exosome component 5 (EXOSC5, also known as RRP46) (27). The ectopic expression of EXOSC5 reduced the level of MLV transcripts in the cytosol (Fig. 5*A*). Under normal conditions, EXOSC5 localized in the cytosol and nuclei, and colocalized with the DCP1A-positive RNA granules at low frequency (Fig. 5*B*). However, when ZAP was ectopically expressed, EXOSC5 moved from the cytosol to the ZAP- and DCP1A-positive RNA granules (Fig. 5*B*). These findings indicate that ZAP recruits the exosome component to the RNA granules to induce the degradation of MLV transcripts.

ZAP Does Not Regulate the RIG-I–Dependent Type I IFN Response in Primary Mouse Cells. A recent study showed that ZAP positively regulated RIG-I signaling during RNA virus infection in a human cell line (28). Therefore, we examined the involvement of ZAP in the RIG-I–dependent type I IFN response in primary mouse cells. In *Zc3hav1*$^{-/-}$ primary MEFs, the IFN-β and Cxcl10 proteins were produced normally in response to VSV, an RNA virus recognized by RIG-I (Fig. 6 *A* and *B*). Although ZAP deficiency greatly enhanced the replication of MLV (Fig. 2 *A* and *B*), no IFN-β or Cxcl10 protein was produced in *Zc3hav1*$^{-/-}$ MEFs infected with MLV. In *Zc3hav1*$^{-/-}$ mouse primary dendritic cells, IFN-β and Cxcl10 were also normally produced in response to

IMMUNOLOGY

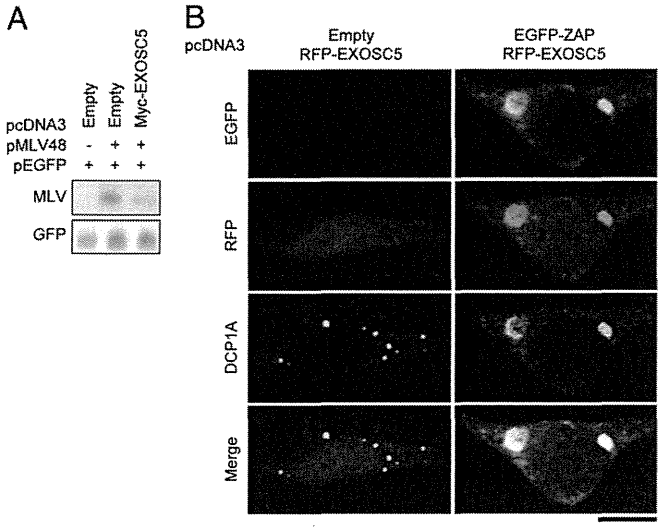

Fig. 5. EXOSC5 colocalizes with ZAP on RNA granules. (*A*) 293T cells were transfected with pMLV-48 and pEGFP-N1 together with the indicated ZAP expression plasmids for 48 h. Cytoplasmic RNA was subjected to Northern blotting analysis to detect the indicated RNAs. (*B*) 293T cells were transfected with the indicated plasmids and then fixed. The samples were immunostained with anti-DCP1A antibody and then observed by confocal laser scanning microscopy. The data are representative of three independent experiments. (Scale bar, 10 μm.)

Newcastle disease virus (NDV) and IAV, RNA viruses recognized by RIG-I (Fig. 6 *C* and *D*). Furthermore, ZAP deficiency did not affect the production of IFN-β in MEFs stimulated with the RIG-I ligand, 5′ triphosphate dsRNA (3pRNA) (Fig. S7 *A* and *B*), the MDA5 ligand poly(rI–rC), and a synthetic dsDNA poly(dA–dT) (Fig. S7*C*). These findings indicate that ZAP is not a regulator of the RIG-I–dependent type I IFN response in primary mouse cells and strengthen our conclusion that ZAP eliminates MLV independently of the RLR–IRF3/7 signaling axis.

Discussion

In this study, we showed that endogenous ZAP suppresses the replication of MLV in MEFs. This raises the issue of whether endogenous ZAP suppresses the replication of other types of RNA viruses, including human retroviruses. The RNAi-mediated knockdown of *ZC3HAV1* mRNA enhanced the replication of xenotropic MLV-related virus, an artificial retrovirus belonging to the gammaretroviral genus of the family *Retroviridae* (29), in 293T cells (Fig. S8 *A* and *B*), whereas the knockdown of *ZC3HAV1* mRNA did not enhance the replication of human T-cell leukemia virus type I, a retrovirus belonging to the deltaretroviral genus of the family *Retroviridae* (30), in MT-2 cells (Fig. S8 *C* and *D*). In a previous study, the knockdown of *ZC3HAV1* mRNA enhanced the replication of HIV-1, a retrovirus belonging to the lentiviral genus of the family *Retroviridae* (31), in HOS-CD4 cells expressing chemokine (C-C motif) receptor 5 (32). Therefore, ZAP functions in human cells to target not all but certain types of retroviruses. ZAP is also known to suppress the replication of RNA viruses belonging to the families *Filoviridae* and *Togaviridae* (33, 34). Although ZAP has been shown to recognize the viral RNA of RNA viruses belonging to the families *Filoviridae*, *Togaviridae*, and *Retroviridae via*, its CCCH-type zinc-finger domains, the common features that are recognized by these domains, such as specific sequences or structural characteristics, have not been determined. Further studies are required to identify the RNA ligand of ZAP that induces the destabilization of the viral RNA by the RNA degradation machinery.

Although accumulating evidence indicates that ZAP counters a variety of RNA viruses under in vitro experimental conditions (20, 33, 34), it is still unclear whether ZAP protects hosts from RNA viral infections in vivo. RNA-sensing TLRs and the ssDNA cytosine deaminase apolipoprotein B mRNA-editing, enzyme-catalytic, polypeptide-like 3 are other antiviral systems that affect mouse retroviruses, and also control the replication of endogenous retroviruses (ERVs) (16, 35–37). Therefore, ZAP might also contribute to the antiviral response to ERVs and prevent the ERV-induced generation of tumors in vivo. To assess this, we are now establishing a colony of *Zc3hav1*$^{-/-}$ mice in the C57BL/6 genetic background. In a future study, we will attempt to determine the in vivo role of ZAP in the host defense responses to endogenous and exogenous microbes.

The CCCH-type zinc-finger–domain-containing protein family regulates RNA synthesis, splicing, and degradation, and is involved in a variety of cellular events, including cell growth, cell death, the inflammatory response, and the antimicrobial response (38, 39). To date, more than 50 CCCH-type zinc-finger-domain–containing proteins have been identified (40). Although various CCCH-type zinc-finger-domain-containing proteins, including tristetraprolin, roquin, and regnase-1, have been shown to be regulators of cytokine mRNA stability, ZAP is the only CCCH-type zinc-finger–domain-containing protein known to promote the destabilization of viral RNA (20, 41–43). Therefore, it will be interesting to identify a CCCH-type zinc-finger–domain-containing protein capable of mediating an antiviral response to RNA viruses that have evaded ZAP and the other RNA-sensing PRRs.

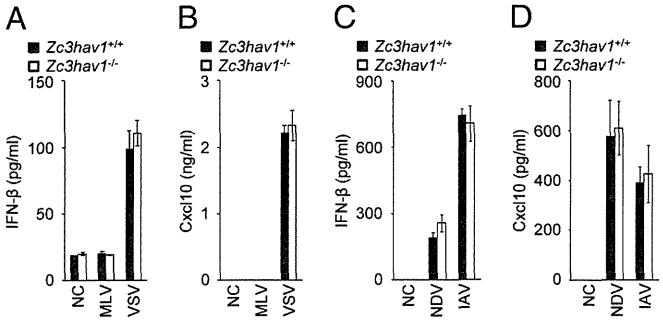

Fig. 6. ZAP is not essential for the RIG-I–mediated type I IFN response. (*A* and *B*) *Zc3hav1*$^{+/+}$ and *Zc3hav1*$^{-/-}$ MEFs were infected with MLV (2×10^{10} copies per μL) or VSV (MOI = 1) for 12 h. The levels of IFN-β (*A*) and Cxcl10 (*B*) proteins in the culture supernatants were measured with ELISAs. (*C* and *D*) *Zc3hav1*$^{+/+}$ and *Zc3hav1*$^{-/-}$ bone marrow-derived dendritic cells were infected with NDV (2.5×10^5 pfu/mL) or IAV (PR8, 100 Hematoglutinin) for 24 h. The levels of IFN-β (*C*) and Cxcl10 (*D*) proteins in the culture supernatants were measured with ELISAs. The results shown are means ± SD ($n = 3$).

Materials and Methods

Reagents. Anti-MLV-Gag antibody (ABIN457547) was purchased from Antibodies-online. Anti–α-tubulin antibody (T6199) was purchased from Sigma. Anti-GFP antibody (598) was purchased from MBL. Chicken anti–avian myelocytomatosis viral oncogene homolog (Myc) antibody (A190-103A) for the immunostaining assay was purchased from Bethyl Laboratories. Mouse anti–Myc-tag antibody (2276S) for immunoblotting was purchased from Cell Signaling. Anti-DDX6 (ab40684), anti-PMP70 (ab3421), and anti-LAMP1 (ab24170) antibodies were purchased from Abcam. Anti-DCP1A antibody (H00055802-M06) was purchased from Abnova. Anti-TOM20 antibody (SC-11415) was purchased from Santa Cruz Biotechnology. Anti-EEA1 antibody (610456) was purchased from BD Biosciences. The ELISA kit for mouse IFN-β was purchased from Pestka Biomedical Laboratories Interferon Source. The ELISA kit for mouse Cxcl10 was purchased from R&D Systems.

Plasmids. pMLV-48 (GenBank accession no. J02255.1) was previously described (44) and kindly donated by H. Fan (University of California, Irvine, CA). pcDNA3.1(+) was purchased from Invitrogen. To generate the ZAP

expression constructs, NheI/NotI cDNA fragments encoding full-length mouse ZAP (GenBank accession no. NM_028864.2) and the C-terminal portion of ZAP and a BamHI/NotI cDNA fragment encoding the N-terminal portion of ZAP were amplified from pCMV–SPORT6–Zc3hav1 (MMM1013-7511214, Open Biosystems) by PCR and cloned into the corresponding restriction sites of pcDNA3 to produce pcDNA3–ZAP, pcDNA3–ZAP–C, and pcDNA3–ZAP–N, respectively. To generate the expression construct for the EGFP–ZAP fusion protein, an NheI/SpeI cDNA fragment encoding EGFP was amplified from pEGFP-N1 (Clontech) by PCR and cloned into the NheI site of pcDNA3–ZAP to produce pcDNA3–EGFP–ZAP. To generate the red fluorescent protein (RFP) expression construct, a BamHI/EcoRI cDNA fragment of RFP was amplified from pTagRFP-N1 (Evrogen) by PCR and cloned into the BamHI/EcoRI sites of pcDNA3 to produce pcDNA3–RFP. To generate the expression constructs for the RFP–DCP1A and RFP–EXOSC5 fusion proteins, EcoRI/NotI cDNA fragments of human DCP1A and human EXOSC5 were amplified from a 293T cDNA library by PCR, and cloned into the EcoRI/NotI sites of pcDNA3–RFP to produce pcDNA3–RFP–DCP1A and pCDNA3–RFP–EXOSC5.

Mice, Cells, and Viruses. C57BL/6 mice were purchased from CLEA Japan, Inc. *Irf3*$^{-/-}$*/Irf7*$^{-/-}$ mice were kindly donated by T. Taniguchi (The University of Tokyo, Tokyo, Japan). The *Ddx58*$^{-/-}$*/Ifih1*$^{-/-}$ mice have been described previously (45). The mice were maintained in our animal facility and treated in accordance with the guidelines of Osaka University. Primary MEFs were prepared from pregnant female mice on embryonic day 13.5, as described previously (4). To prepare bone marrow-derived dendritic cells, mouse bone marrow cells were cultured in the presence of 10 ng/mL GM-CSF (PeproTech) for 6 d, during which time the culture medium was replaced with medium containing GM-CSF every 2 d. The 293T cells have been described previously (46). Replication-competent MLV was produced by 293T cells transfected with pMLV-48. To induce infection, MLV was incubated with MEFs for 2 h in the presence of 10 μg/mL Polybrene (Millipore). VSV, IAV (A/Puerto Rico/8/34, H1N1 strain), and NDV have been described elsewhere (3, 4).

Quantitative RT-PCR. Total RNA was isolated using the ZR RNA MicroPrep kit (Zymo Research), according the manufacturer's instructions. Viral RNA was isolated from the culture supernatants using the ZR Viral RNA kit (Zymo Research), according the manufacturer's instructions. RT was performed using random primers and Verso reverse transcriptase (Thermo Scientific) according to the manufacturer's instructions. For quantitative PCR, the cDNA fragments were amplified from the RT products with Real-Time PCR Master Mix (Toyobo) according to the manufacturer's instructions. The fluorescence from the TaqMan probe for each cytokine was detected with a 7500 Real-Time PCR System (Applied Biosystems). To determine the relative induction of cytokine mRNAs, the level of mRNA expressed from each gene was normalized to the expression of 18S RNA. The copy number of the MLV genomic RNA was determined with the dsDNA copy number calculator program. The experiments were repeated at least three times, with reproducible results.

ELISAs. The levels of IFN-β and Cxcl10 in the culture supernatants were measured with ELISAs in accordance with the manufacturer's instructions. The experiments were repeated at least three times, with reproducible results.

Northern Blotting. Cytoplasmic RNA was extracted using the Cytoplasmic and Nuclear RNA Purification Kit (Norgen) according the manufacturer's instructions. The RNA obtained was separated electrophoretically, transferred to nylon membranes, and hybridized with the indicated probes. An RNA probe was designed to hybridize specifically to the Gag region from nucleotide 1291 to nucleotide 1472 of the MLV transcripts. The experiments were repeated at least three times, with reproducible results.

Immunoblotting. Immunoblotting was performed as described previously (47). The experiments were repeated at least three times, with reproducible results.

Immunostaining Assay. Cells cultured in microscopy chambers (ibidi) were fixed with 3% (wt/vol) paraformaldehyde and then processed for immunostaining as described previously (47). The samples were examined under an LSM 780 confocal laser scanning microscope (Carl Zeiss). The experiments were repeated at least three times, with reproducible results.

Detection of the MLV Transcripts with FISH. The cells were fixed with 4% paraformaldehyde. FISH was performed using the QuantiGene ViewRNA ISH Cell Assay kit (Veritas) according to the manufacturer's instructions. A Cy5-labeled FISH probe was designed to hybridize specifically to the Gag region from nucleotide 607 to nucleotide 1833 of the MLV transcripts. The samples were examined under an LSM780 confocal laser scanning microscope. The experiments were repeated at least three times, with reproducible results.

ACKNOWLEDGMENTS. We thank Drs. H. Fan, D. Trono, H. Miyoshi, and T. Taniguchi for providing invaluable materials and the members of the Laboratory of Host Defenses for their assistance. This work was supported by a Japan Society for the Promotion of Science Grant-in-Aid for Challenging Exploratory Research (to T. Saitoh); the Cabinet Office, Government of Japan, and the Japan Society for the Promotion of Science Funding Program for World-Leading Innovative Research and Development on Science and Technology "FIRST Program" (to S.A.); and National Institutes of Health Grant P01-AI070167 (to S.A.).

1. Kawai T, Akira S (2009) The roles of TLRs, RLRs and NLRs in pathogen recognition. *Int Immunol* 21(4):317–337.
2. Iwasaki A (2012) A virological view of innate immune recognition. *Annu Rev Microbiol* 66:177–196.
3. Yoneyama M, et al. (2004) The RNA helicase RIG-I has an essential function in double-stranded RNA-induced innate antiviral responses. *Nat Immunol* 5(7):730–737.
4. Kato H, et al. (2006) Differential roles of MDA5 and RIG-I helicases in the recognition of RNA viruses. *Nature* 441(7089):101–105.
5. Yoneyama M, et al. (1998) Direct triggering of the type I interferon system by virus infection: Activation of a transcription factor complex containing IRF-3 and CBP/p300. *EMBO J* 17(4):1087–1095.
6. Honda K, et al. (2005) IRF-7 is the master regulator of type-I interferon-dependent immune responses. *Nature* 434(7034):772–777.
7. Alexopoulou L, Holt AC, Medzhitov R, Flavell RA (2001) Recognition of double-stranded RNA and activation of NF-kappaB by Toll-like receptor 3. *Nature* 413(6857): 732–738.
8. Yamamoto M, et al. (2003) Role of adaptor TRIF in the MyD88-independent toll-like receptor signaling pathway. *Science* 301(5633):640–643.
9. Cella M, et al. (1999) Plasmacytoid monocytes migrate to inflamed lymph nodes and produce large amounts of type I interferon. *Nat Med* 5(8):919–923.
10. Diebold SS, Kaisho T, Hemmi H, Akira S, Reis e Sousa C (2004) Innate antiviral responses by means of TLR7-mediated recognition of single-stranded RNA. *Science* 303(5663):1529–1531.
11. Heil F, et al. (2004) Species-specific recognition of single-stranded RNA via toll-like receptor 7 and 8. *Science* 303(5663):1526–1529.
12. Kawai T, et al. (2004) Interferon-alpha induction through Toll-like receptors involves a direct interaction of IRF7 with MyD88 and TRAF6. *Nat Immunol* 5(10):1061–1068.
13. Honda K, et al. (2005) Spatiotemporal regulation of MyD88-IRF-7 signalling for robust type-I interferon induction. *Nature* 434(7036):1035–1040.
14. Ihle JN, Rein A, Mural R (1984) Immunological and virological mechanisms in retrovirus-induced murine leukemogenesis. *Advances in Viral Oncology*, ed Klein G (Raven Press, New York), pp 95–137.
15. Schiff RD, Oliff A (1986) The pathophysiology of murine retrovirus-induced leukemias. *Crit Rev Oncol Hematol* 5(3):257–323.
16. Kane M, et al. (2011) Innate immune sensing of retroviral infection via Toll-like receptor 7 occurs upon viral entry. *Immunity* 35(1):135–145.
17. Everitt AR, et al.; GenISIS Investigators; MOSAIC Investigators (2012) IFITM3 restricts the morbidity and mortality associated with influenza. *Nature* 484(7395):519–523.
18. Fensterl V, et al. (2012) Interferon-induced Ifit2/ISG54 protects mice from lethal VSV neuropathogenesis. *PLoS Pathog* 8(5):e1002712.
19. Goubau D, Deddouche S, Reis E Sousa C (2013) Cytosolic sensing of viruses. *Immunity* 38(5):855–869.
20. Gao G, Guo X, Goff SP (2002) Inhibition of retroviral RNA production by ZAP, a CCCH-type zinc finger protein. *Science* 297(5587):1703–1706.
21. Guo X, Carroll JW, Macdonald MR, Goff SP, Gao G (2004) The zinc finger antiviral protein directly binds to specific viral mRNAs through the CCCH zinc finger motifs. *J Virol* 78(23):12781–12787.
22. Guo X, Ma J, Sun J, Gao G (2007) The zinc-finger antiviral protein recruits the RNA processing exosome to degrade the target mRNA. *Proc Natl Acad Sci USA* 104(1): 151–156.
23. Chen G, Guo X, Lv F, Xu Y, Gao G (2008) p72 DEAD box RNA helicase is required for optimal function of the zinc-finger antiviral protein. *Proc Natl Acad Sci USA* 105(11): 4352–4357.
24. Ye P, Liu S, Zhu Y, Chen G, Gao G (2010) DEXH-Box protein DHX30 is required for optimal function of the zinc-finger antiviral protein. *Protein Cell* 1(10):956–964.
25. Wang X, Lv F, Gao G (2010) Mutagenesis analysis of the zinc-finger antiviral protein. *Retrovirology* 7:19.
26. Reineke LC, Lloyd RE (2013) Diversion of stress granules and P-bodies during viral infection. *Virology* 436(2):255–267.
27. Liu Q, Greimann JC, Lima CD (2006) Reconstitution, activities, and structure of the eukaryotic RNA exosome. *Cell* 127(6):1223–1237.
28. Hayakawa S, et al. (2011) ZAPS is a potent stimulator of signaling mediated by the RNA helicase RIG-I during antiviral responses. *Nat Immunol* 12(1):37–44.
29. Paprotka T, et al. (2011) Recombinant origin of the retrovirus XMRV. *Science* 333(6038):97–101.
30. Yamamoto N, Hinuma Y (1985) Viral aetiology of adult T-cell leukaemia. *J Gen Virol* 66(Pt 8):1641–1660.

31. Haseltine WA (1988) Replication and pathogenesis of the AIDS virus. *J Acquir Immune Defic Syndr* 1(3):217–240.
32. Zhu Y, et al. (2011) Zinc-finger antiviral protein inhibits HIV-1 infection by selectively targeting multiply spliced viral mRNAs for degradation. *Proc Natl Acad Sci USA* 108(38):15834–15839.
33. Müller S, et al. (2007) Inhibition of filovirus replication by the zinc finger antiviral protein. *J Virol* 81(5):2391–2400.
34. Bick MJ, et al. (2003) Expression of the zinc-finger antiviral protein inhibits alphavirus replication. *J Virol* 77(21):11555–11562.
35. Okeoma CM, Lovsin N, Peterlin BM, Ross SR (2007) APOBEC3 inhibits mouse mammary tumour virus replication in vivo. *Nature* 445(7130):927–930.
36. Santiago ML, et al. (2008) Apobec3 encodes Rfv3, a gene influencing neutralizing antibody control of retrovirus infection. *Science* 321(5894):1343–1346.
37. Yu P, et al. (2012) Nucleic acid-sensing Toll-like receptors are essential for the control of endogenous retrovirus viremia and ERV-induced tumors. *Immunity* 37(5):867–879.
38. Chen CY, et al. (2001) AU binding proteins recruit the exosome to degrade ARE-containing mRNAs. *Cell* 107(4):451–464.
39. Hurt JA, et al. (2009) A conserved CCCH-type zinc finger protein regulates mRNA nuclear adenylation and export. *J Cell Biol* 185(2):265–277.
40. Liang J, Song W, Tromp G, Kolattukudy PE, Fu M (2008) Genome-wide survey and expression profiling of CCCH-zinc finger family reveals a functional module in macrophage activation. *PLoS ONE* 3(8):e2880.
41. Lai WS, et al. (1999) Evidence that tristetraprolin binds to AU-rich elements and promotes the deadenylation and destabilization of tumor necrosis factor alpha mRNA. *Mol Cell Biol* 19(6):4311–4323.
42. Yu D, et al. (2007) Roquin represses autoimmunity by limiting inducible T-cell costimulator messenger RNA. *Nature* 450(7167):299–303.
43. Matsushita K, et al. (2009) Zc3h12a is an RNase essential for controlling immune responses by regulating mRNA decay. *Nature* 458(7242):1185–1190.
44. Bacheler L, Fan H (1981) Isolation of recombinant DNA clones carrying complete integrated proviruses of Moloney murine leukemia virus. *J Virol* 37(1):181–190.
45. Kato H, et al. (2008) Length-dependent recognition of double-stranded ribonucleic acids by retinoic acid-inducible gene-I and melanoma differentiation-associated gene 5. *J Exp Med* 205(7):1601–1610.
46. Saitoh Y, et al. (2008) Overexpressed NF-kappaB-inducing kinase contributes to the tumorigenesis of adult T-cell leukemia and Hodgkin Reed-Sternberg cells. *Blood* 111(10):5118–5129.
47. Saitoh T, et al. (2008) Loss of the autophagy protein Atg16L1 enhances endotoxin-induced IL-1beta production. *Nature* 456(7219):264–268.

HEPATOLOGY
Official Journal of the American Association for the Study of Liver Diseases

Human Blood Dendritic Cell Antigen 3 (BDCA3)$^+$ Dendritic Cells Are a Potent Producer of Interferon-λ in Response to Hepatitis C Virus

Sachiyo Yoshio,[1] Tatsuya Kanto,[1] Shoko Kuroda,[1] Tokuhiro Matsubara,[1] Koyo Higashitani,[1] Naruyasu Kakita,[1] Hisashi Ishida,[1] Naoki Hiramatsu,[1] Hiroaki Nagano,[2] Masaya Sugiyama,[3] Kazumoto Murata,[3] Takasuke Fukuhara,[4] Yoshiharu Matsuura,[4] Norio Hayashi,[5] Masashi Mizokami,[3] and Tetsuo Takehara[1]

The polymorphisms in the interleukin (*IL*)-*28B* (interferon-lambda [IFN]-λ3) gene are strongly associated with the efficacy of hepatitis C virus (HCV) clearance. Dendritic cells (DCs) sense HCV and produce IFNs, thereby playing some cooperative roles with HCV-infected hepatocytes in the induction of interferon-stimulated genes (ISGs). Blood dendritic cell antigen 3 (BDCA3)$^+$ DCs were discovered as a producer of IFN-λ upon Toll-like receptor 3 (TLR3) stimulation. We thus aimed to clarify the roles of BDCA3$^+$ DCs in anti-HCV innate immunity. Seventy healthy subjects and 20 patients with liver tumors were enrolled. BDCA3$^+$ DCs, in comparison with plasmacytoid DCs and myeloid DCs, were stimulated with TLR agonists, cell-cultured HCV (HCVcc), or Huh7.5.1 cells transfected with HCV/JFH-1. BDCA3$^+$ DCs were treated with anti-CD81 antibody, inhibitors of endosome acidification, TIR-domain-containing adapter-inducing interferon-β (TRIF)-specific inhibitor, or ultraviolet-irradiated HCVcc. The amounts of IL-29/IFN-λ1, IL-28A/IFN-λ2, and IL-28B were quantified by subtype-specific enzyme-linked immunosorbent assay (ELISA). The frequency of BDCA3$^+$ DCs in peripheral blood mononuclear cell (PBMC) was extremely low but higher in the liver. BDCA3$^+$ DCs recovered from PBMC or the liver released large amounts of IFN-λs, when stimulated with HCVcc or HCV-transfected Huh7.5.1. BDCA3$^+$ DCs were able to induce ISGs in the coexisting JFH-1-positive Huh7.5.1 cells. The treatments of BDCA3$^+$ DCs with anti-CD81 antibody, cloroquine, or bafilomycin A1 reduced HCVcc-induced IL-28B release, whereas BDCA3$^+$ DCs comparably produced IL-28B upon replication-defective HCVcc. The TRIF-specific inhibitor reduced IL-28B release from HCVcc-stimulated BDCA3$^+$ DCs. In response to HCVcc or JFH-1-Huh7.5.1, BDCA3$^+$ DCs in healthy subjects with IL-28B major (rs8099917, TT) released more IL-28B than those with IL-28B minor genotype (TG). *Conclusion*: Human BDCA3$^+$ DCs, having a tendency to accumulate in the liver, recognize HCV in a CD81-, endosome-, and TRIF-dependent manner and produce substantial amounts of IL-28B/IFN-λ3, the ability of which is superior in subjects with IL-28B major genotype. (HEPATOLOGY 2013;57:1705-1715)

Hepatitis C virus (HCV) infection is one of the most serious health problems in the world. More than 170 million people are chronically infected with HCV and are at high risk of developing liver cirrhosis and hepatocellular carcinoma. Genome-wide association studies have successfully identified the genetic polymorphisms (single nucleotide polymorphisms, SNPs) upstream of the promoter region of the

Abbreviations: Ab, antibody; HCV, hepatitis C virus; HCVcc, cell-cultured hepatitis C virus; HSV, herpes simplex virus; IHL, intrahepatic lymphocyte; INF-λ, interferon-lambda; IRF, interferon regulatory factor; ISGs, interferon-stimulated genes; JEV, Japanese encephalitis virus; Lin, lineage; mDC, myeloid DC; MOI, multiplicity of infection; PBMC, peripheral blood mononuclear cell; pDC, plasmacytoid DC; Poly IC, polyinosine-polycytidylic acid; RIG-I, retinoic acid-inducible gene-I; SNPs, single nucleotide polymorphisms; TLR, Toll-like receptor; TRIF, TIR-domain-containing adapter-inducing interferon-β.

From the [1]Department of Gastroenterology and Hepatology, Osaka University Graduate School of Medicine, Osaka, Japan; [2]Department of Surgery, Osaka University Graduate School of Medicine, Osaka, Japan; [3]Research Center for Hepatitis and Immunology, National Center for Global Health and Medicine, Ichikawa, Japan; [4]Department of Molecular Virology, Research Institute for Microbial Diseases, Osaka University, Osaka, Japan; [5]Kansai Rosai Hospital, Hyogo, Japan.

Received July 2, 2012; accepted November 13, 2012.

Supported in part by a Grant-In-Aid for Scientific Research from the Ministry of Education, Culture, Sports, Science, and Technology, Japan and a Grant-In-Aid from the Ministry of Health, Labor, and Welfare of Japan.